

UNCLASSIFIED

AD NUMBER

AD529359

LIMITATION CHANGES

TO:

Approved for public release; distribution is unlimited.

FROM:

Distribution authorized to U.S. Gov't. agencies and their contractors;
Administrative/Operational Use; DEC 1973. Other requests shall be referred to Defense Advanced Research Projects Agency, Washington, DC 20301.

AUTHORITY

radc ltr 16 Jul 1974

THIS PAGE IS UNCLASSIFIED

UNCLASSIFIED

AD 529359

CLASSIFICATION CHANGED
TO: UNCLASSIFIED
FROM: ~~SECRET~~
AUTHORITY:

 RADC, USAF
 ITR, 16 JUL 74

UNCLASSIFIED

SECRET

AD529359

RADC-TR-74-45
Final Technical Report
15 December 1973

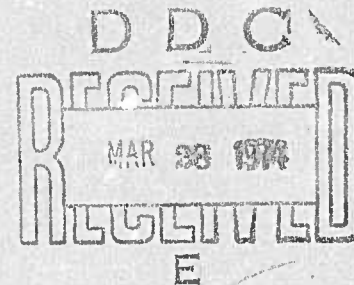


EXPERIMENTS AND MODELS IN PRAIRIE SMOKE (U)

Aeronomy Corporation

**Sponsored By
Defense Advanced Research Projects Agency
ARPA Order No. 1423**

**NATIONAL SECURITY INFORMATION
Unauthorized Disclosure Subject To
Criminal Sanctions**



The views and conclusions contained in this document are those of the authors and should not be interpreted as necessarily representing the official policies, either expressed or implied, of the Defense Advanced Research Projects Agency or the U. S. Government.

Rome Air Development Center
Air Force Systems Command
Griffiss Air Force Base, New York

SECRET

**DDC CONTROL
NO. 40673**

13

Do not return this copy, when no longer needed destroy in accordance with pertinent security regulations.

11

SECRET

EXPERIMENTS AND MODELS IN PRAIRIE SMOKE (U)

S. A. Bowhill
E. K. Walton
D. R. Ward

Contractor: Aeronomy Corporation
Contract Number: F30602-72-C-0214
Effective Date of Contract: 1 September 1971
Contract Expiration Date: 31 October 1973
Amount of Contract: \$227,120.00
Program Code Number: 1E20

Principal Investigator: Dr. S. A. Bowhill
Phone: 217 359-8007

Project Engineer: Vincent J. Coyne
Phone: 315 330-3141

Contract Engineer: Richard W. Carman
Phone: 315 330-3144

This research was supported by the
Defense Advanced Research Projects
Agency of the Department of Defense
and was monitored by Richard Carman
RADC (OCSE), GAFB, NY 13441 under
contract F30602-72-C-0214.

CLASSIFIED BY: Ivory Coral Sec. Guide
EXEMPT FROM GENERAL DECLASSIFICATION
SCHEDULE OF EXECUTIVE ORDER 11652
EXEMPTION CATEGORY: 3
DECLASSIFY ON 31 Dec 84.

#296


Copy 17 of 17 copies

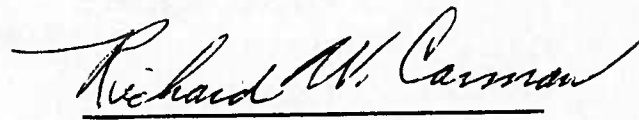
SECRET

DOC CONTROL
NO. 10673

PUBLICATION REVIEW

This technical report has been reviewed and is approved.


RADC Project Engineer


RADC Contract Engineer

SECRET

ABSTRACT (U)

(S) This final report describes additional experiments to study the morphology of artificial spread F (ASF) irregularities by measuring the scintillation of VHF and UHF signals transmitted through the disturbed region from geostationary and orbital satellites. Scintillation depth, structure size and drift velocity measurements are described for Prairie Smoke IV, and are related to heater power. Detailed correlation analysis shows the presence of a smaller structure in ASF of about 10 meter size. The results of these experiments are combined into a model for scintillation and spread F. The report also contains recommendations on the effect of antenna power patterns and beam steering on field-aligned VHF scatter; and on models for D-region absorption.

SECRET

SECRET

TABLE OF CONTENTS (U)

ABSTRACT (U)	iii
1. INTRODUCTION AND SUMMARY OF PREVIOUS WORK (U)	1
2. GEOSTATIONARY TRANSMISSION EXPERIMENTS IN PRAIRIE SMOKE IV (U)	4
2.1 Introduction (U)	4
2.2 Experimental observations (U)	4
3. YIELD STUDIES BASED ON GEOSTATIONARY SATELLITE TRANSMISSIONS (U)	15
3.1 Introduction (U)	15
3.2 Data analysis (U)	15
4. CORRELATION ANALYSIS OF PRAIRIE SMOKE TRANSMISSION RESULTS (U)	21
4.1 Introduction (U)	21
4.2 Irregularity orientation in Prairie Smoke Ib (U)	21
4.3 Irregularity characteristics in Prairie Smoke III (U)	30
5. MODEL FOR SCINTILLATION AND SPREAD F (U)	36
5.1 Description of artificial field-aligned irregularities (U)	36
5.2 Natural spread F (U)	36
5.3 Artificial spread F (U)	37
5.4 Analytical model for ASF (U)	38
6. THE INCLUSION OF ANTENNA POWER PATTERNS IN THE SCATTERING MODEL (U)	41
6.1 Introduction (U)	41
6.2 Antenna polar diagrams (U)	41
6.3 Relative cross sections (U)	51
7. MODELS FOR D-REGION ABSORPTION (U)	63
7.1 Introduction (U)	63
7.2 Electron-density data (U)	63
7.3 One-way absorption (U)	63
8. CONCLUSIONS (U)	68
8.1 Conclusions from scintillation measurements (U)	68
8.2 Conclusions from OFS studies (U)	69
9. REFERENCES (U)	71

SECRET

SECRET

1. INTRODUCTION AND SUMMARY OF PREVIOUS WORK (U)

(S) The purpose of the transmission experiment is to determine the configuration, spatial extent, and time behavior of artificial spread F (ASF) irregularities produced by radio-frequency heating of the ionosphere. The large-scale structure of ASF was first evident on ionosonde records (Utlaut, 1970). The general appearance is similar to that of naturally-occurring spread F, appearing as additional diffuse returns spreading upwards from the ordinary and extraordinary traces over a range difference up to 100 km. It is difficult to determine the spatial characteristics of these irregularities using monostatic measurements from the ground at HF, due to the presence of multipath interference between reflections from different parts of the disturbed region. However, by transmitting a VHF radio signal through the disturbed region, and choosing a frequency sufficiently high that multipath effects are avoided, a rather clear picture of the irregularities can be provided.

(S) The transmission experiment is designed to study ASF by examining amplitude fluctuations from orbiting and geostationary satellite signals received at VHF and UHF by receivers spaced at fixed locations on the ground. The transmission experiment has the following advantages for the study of ionospheric irregularities:

1. The location of the transmitting satellite is accurately known, and the frequencies are sufficiently high for ionospheric refraction to be neglected; so the position of the line of sight (LOS) is accurately predetermined.
2. The ground receiving site can be located so that the LOS passes through any desired part of the disturbed volume.
3. Orbital satellites have a LOS that traverses the disturbed region so rapidly that internal motions of the plasma are negligible as

SECRET

SECRET

a factor in producing amplitude scintillations.

4. For irregularities with correlation distances of 200 m or less, the fluctuations in phase, produced by passage of VLF waves through ASF, are fully developed into amplitude scintillations by the time they reach the ground, so that the phase scintillation fluctuation can be deduced from the depth of amplitude fluctuation.
5. The propagation of VHF and UHF waves through the disturbed region is of inherent interest for some propagation applications of ASF; for instance, degradation of radar tracking of orbiting or ballistic missiles.

(S) It is important to realize the distinction between the forward scattering phenomenon studied by the transmission experiment, which occurs at all angles to the magnetic field (but most intensely nearly along the field) and the radar backscattering from smaller-scale irregularities (significant primarily for directions nearly normal to the magnetic field).

(S) In the first report under this contract (RADC-TR-72-200, April 1972) results were described of three-receiver measurements on geostationary and orbital satellites at a fixed location in Prairie Smoke I and the general features of artificial spread F were defined. In the second report (RADC-TR-73-94, October 1972) results were described from Prairie Smoke Ib and II, using mobile geostationary and orbital receiving stations, and using them to map the horizontal extent and altitude distribution of the ASF irregularities. A scattering model for ASF was presented together with a simple model for OFS. In the third report (RADC-TR-73-210, April 1973) experiments were described to study the structure size and time dependence of scintillations from ASF at frequencies of 30, 50, 150 and 400 MHz using digital and analog data recording. Aircraft and topside sounder diagnostics were described to map the vertical and horizontal extent of the disturbed region. Further work was described on optimization of bistatic

SECRET

SECRET

geometry for OFS (on-frequency scatter).

(S) In Section 2 of this report, geostationary transmission experiments are described from Prairie Smoke IV, giving some information as to the variation of scintillation yield with heater frequency. In Section 3 detailed results from Prairie Smoke II are described showing the variation of scintillation with power and time of day. Section 4 describes some new results on the structure size of ASF, including accurate measurements of axis orientation and orbital studies of fine structure. These results are combined in Section 5 into an overall model for ASF. Sections 6 and 7 describe two pieces of work connected with the OFS model; the effect of beam steering (Section 6) and possible magnitudes for D-region absorption (Section 7).

SECRET

SECRET

2. GEOSTATIONARY TRANSMISSION EXPERIMENTS IN PRAIRIE SMOKE IV (U)

2.1 Introduction (U)

(S) The planned scenario for Aeronomy Corporation participation in Prairie Smoke IV called for continuous monitoring of scintillations from the disturbed region over Platteville of a geostationary satellite, permitting time variations of the scintillation index to be followed continuously. In addition to this fixed station observed at 137 MHz, it was planned to use a mobile station in two modes. In the first week, it was to gather geostationary data simultaneously with the fixed station, but at sites displaced at varying distances to the west and south, in order to map the time behavior of various parts of the disturbed region. In the second week, the mobile station was to move to New Mexico to measure the rise and set of orbiting satellites behind the disturbed region in the north, with the objective of measuring the altitude distribution of the irregularities.

(S) Unfortunately, extremely severe weather conditions were encountered at the field stations in Wyoming, consisting of very heavy snow followed by record low temperatures for the late November-early December period. The effects of these conditions were three-fold: disruption of the transmitter schedule; immobilization of the mobile field station; and equipment difficulties resulting from the extremely low temperatures (typically -30 F) exceeding the environmental specifications of the recording instrumentation. Nevertheless, a limited amount of experimental data was obtained, which is described in the next section.

2.2 Experimental observations (U)

(S) The geostationary observing station was set up on the Hoblit ranch near Lusk, Wyoming. This location was chosen because it yields a LOS through the region of interest to the ATS V satellite, and because there

SECRET

SECRET

is an east-west road available for the mobile station to take records to either side of the central fixed station.

(S) The central observing site consisted of three spaced antennas in a right triangle configuration with the 500-ft legs of the triangle oriented north-south and east-west. Three types of recording were used. The product detector outputs of the three receivers were recorded on a 4-track Sony type 366 tape recorder with WWV on the fourth channel for timing purposes. The detected output of each receiver was filtered through a low-pass RC filter ($\tau \sim 1$ sec) and displayed for two antennas on a chart recorder for real-time observation. All three filtered signals were digitized and recorded by a Metrodata DL-616 tape cartridge recorder unit, which was read at a later time for processing by computer. This unit samples at 10 channels/sec and is switchable for 1, 2, 4, 8, or 16 channels. For these observations the unit was adjusted for four channels yielding five samples of each channel every two seconds.

(S) The schedule of observations obtained is shown in Table 2.1. The most complete records were obtained during the first week (November 28-December 1) before the extremely cold weather. However, the second week (December 4-December 8) was hampered by bitter cold and resulting equipment difficulties, and the records were not complete. A summary of transmitter operations and station operations is shown in the table.

(S) Routine operation was followed once the equipment was set up on November 28. On Friday December 1 an orbital pass was scheduled at ~ 1330 MST. No scintillation was observed and the transmitter log revealed that the heater frequency was about 10 percent above foF2 around the time of interest.

(S) The second week yielded few usable records because much of the equipment operated at reduced efficiency; for example, the preamplifiers at the

SECRET

SECRET

Table 2.1

Geostationary transmission experiment schedule in Prairie Smoke IV

Date	Heater transmitter times (MST)	Recording times (MST)	Quality of Records
November 29	1100-1700	1300-1700	Good
November 30	0900-1400	1300-1400	Good
December 1	1100-1400	1230-1400	Poor
December 4	1130-1700	None	None
December 5	0930-1400	1430-1500	Poor
December 6	0900-1700	1345-1545	Good
December 7	1000-1700	1300-1600	Fair
December 8	0930-1700	None	None

SECRET

SECRET

three antennas lost considerable gain because the batteries were freezing. Even with continuous operation of the trailer furnace, a temperature of less than 40° F was maintained, resulting in numerous equipment difficulties.

(S) Analysis has concentrated on the digital tape records obtained during the first week of Prairie Smoke IV. For this purpose, software was developed to read the digital data into the PDP-8e computer and record the data onto DECTape. The advantage of storing on DECTape is that the data are easily accessible for reduction; the Metrodata tape cartridges are continuous-loop type and can be read in the forward direction only. This forward read is not readily adaptable to some processing algorithms such as auto- and cross-correlation, and therefore some other storage such as on DECTape is desirable. The data were transferred onto DECTape in 5-minute intervals for each antenna, and the scintillation index, S , was calculated for each minute. The results are plotted for November 29 and November 30 on Figures 2.1 and 2.2. The parameters of transmitter operation, namely power and $f_H/foF2$, are shown on the same time axis to facilitate comparison. The scintillation index is determined from the amplitude measurements A by the expression

$$\langle A^2 \rangle / \langle A \rangle^2 = S^2 + 1 .$$

(S) The interpretation of these data is quite straightforward. The scintillation is clearly strongest when the heater frequency is from 95% to 97% of the F-layer critical frequency; for higher heater frequencies, the scintillation depth drops off extremely rapidly. For frequencies between 85 and 97% of $foF2$, the scintillation index is approximately proportional to the heater power.

(S) A very limited amount of structure size and velocity information is available for November 29 and 30, and is illustrated on Figures 2.3 and 2.4.

SECRET

SECRET

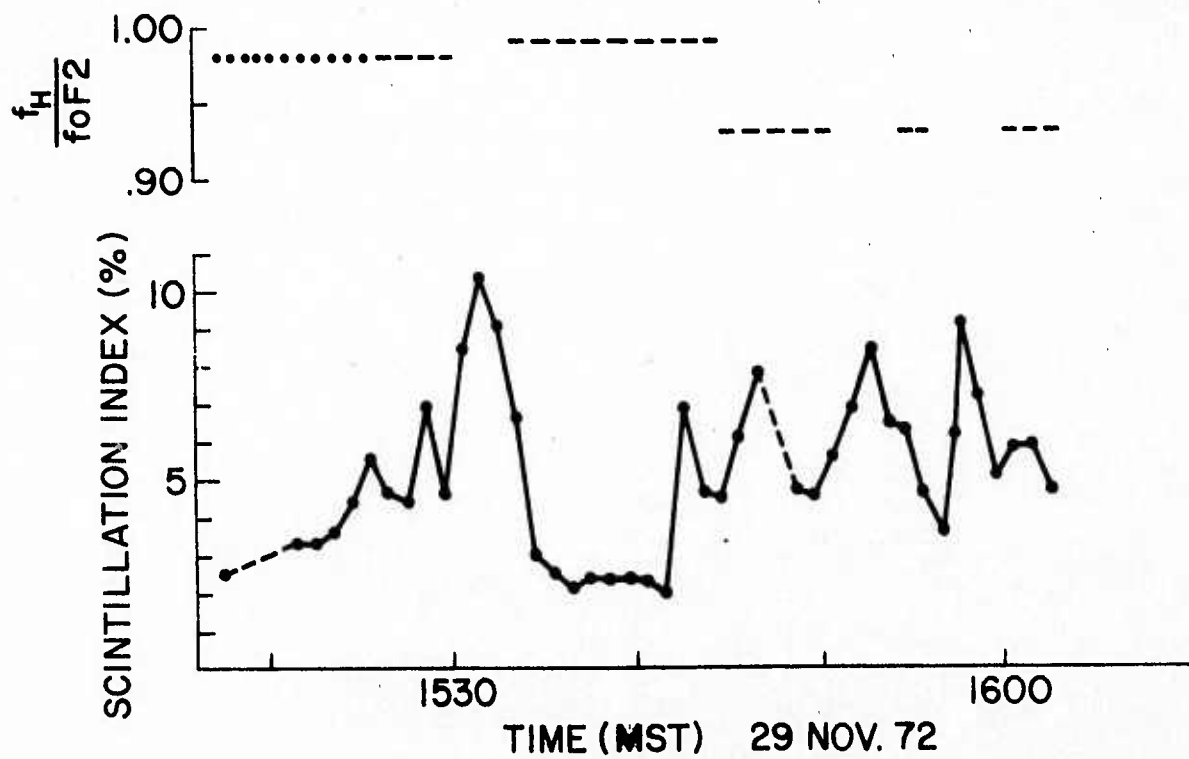
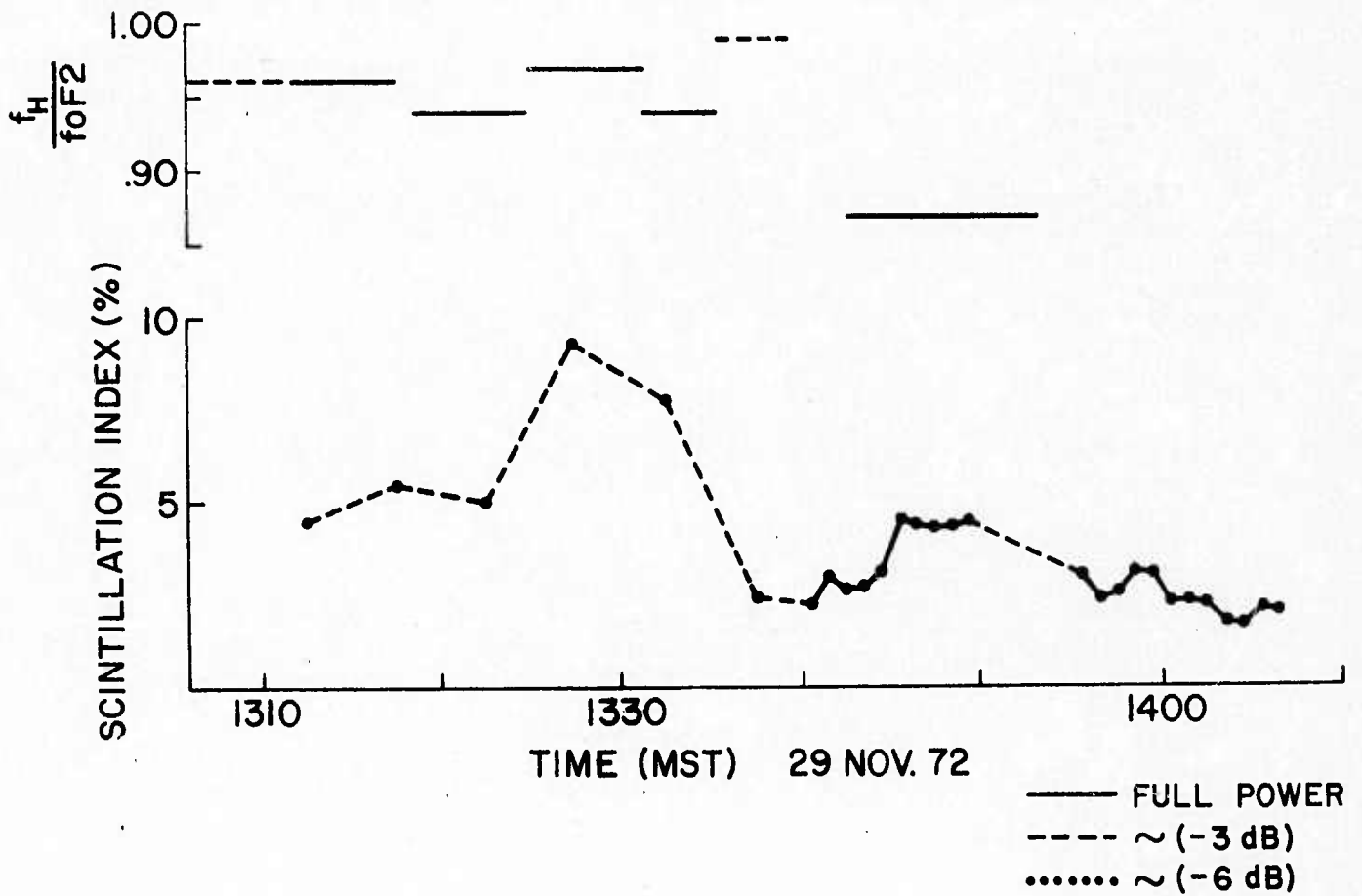


Figure 2.1 Scintillation index for Prairie Smoke IV (U)

SECRET

SECRET

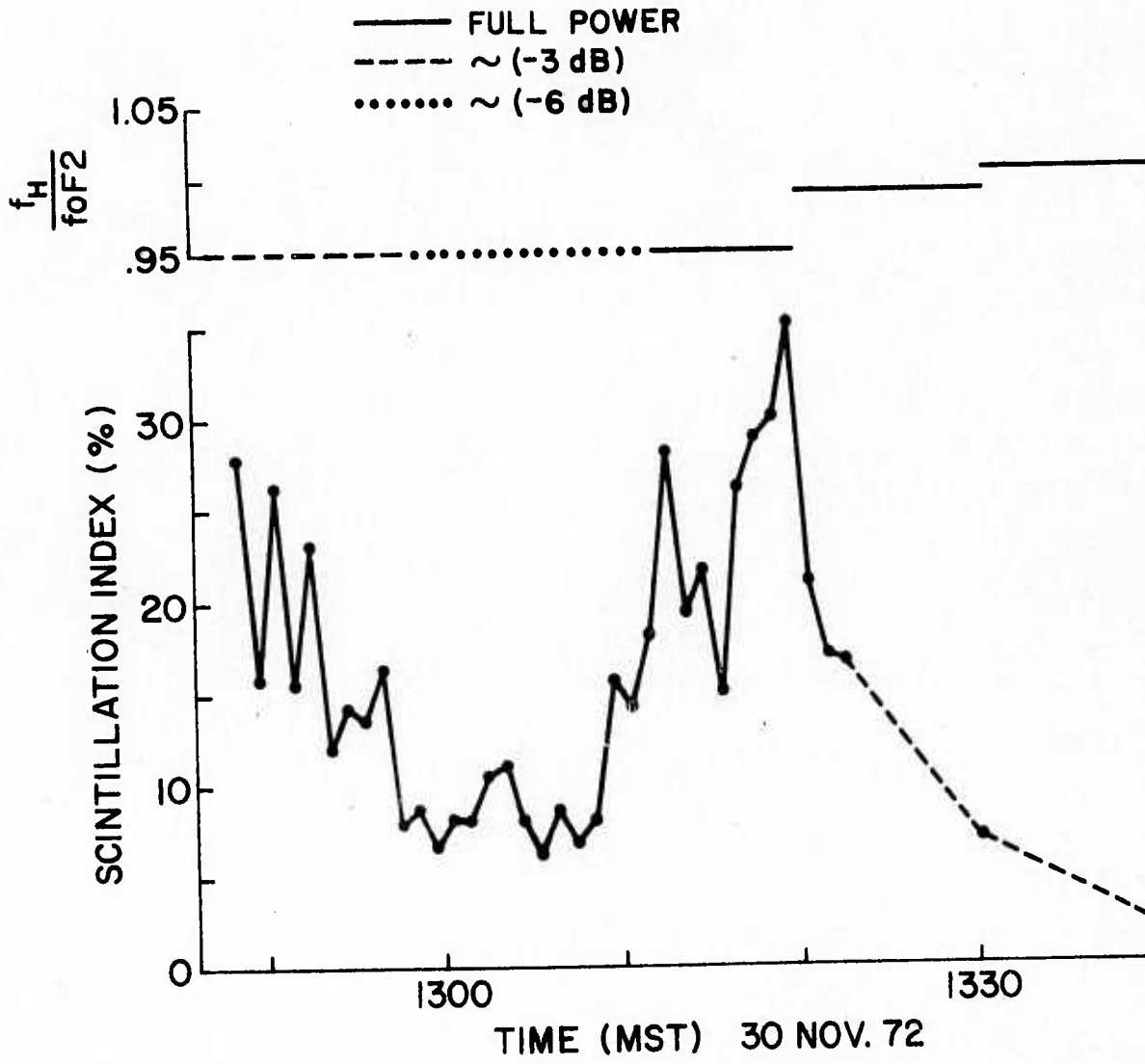


Figure 2.2 Scintillation index for Prairie Smoke IV, continued (U)

SECRET

SECRET

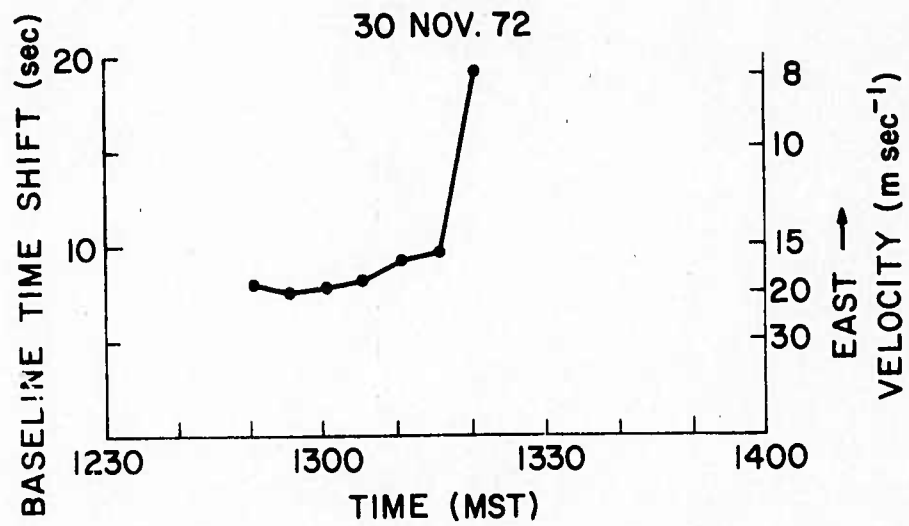
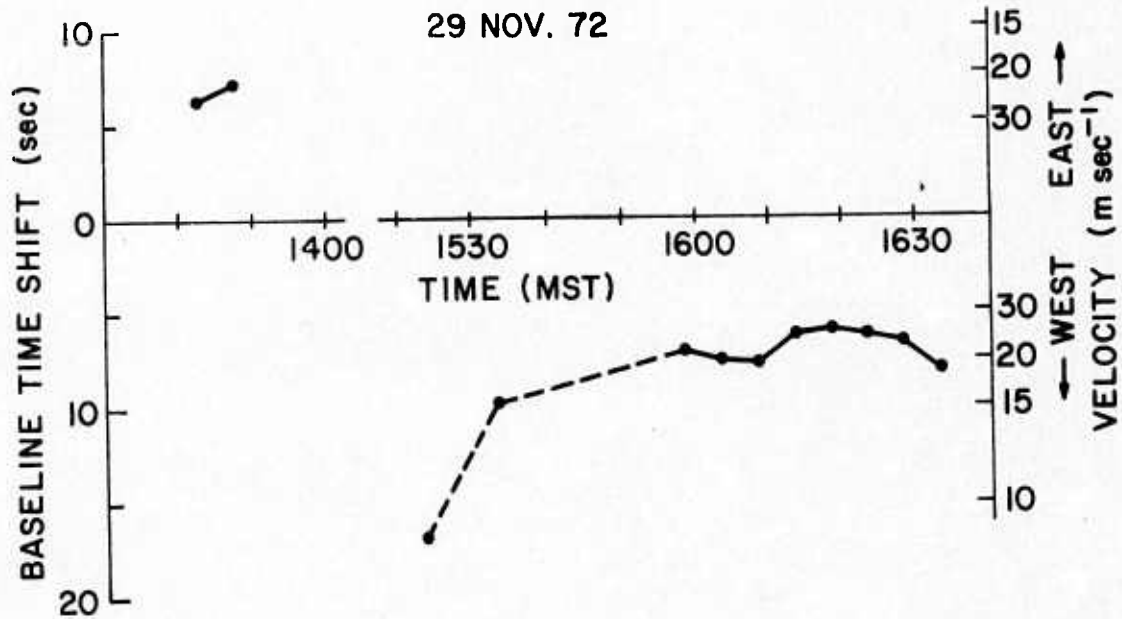


Figure 2.3 Drift velocities for Prairie Smoke IV (U)

SECRET

SECRET

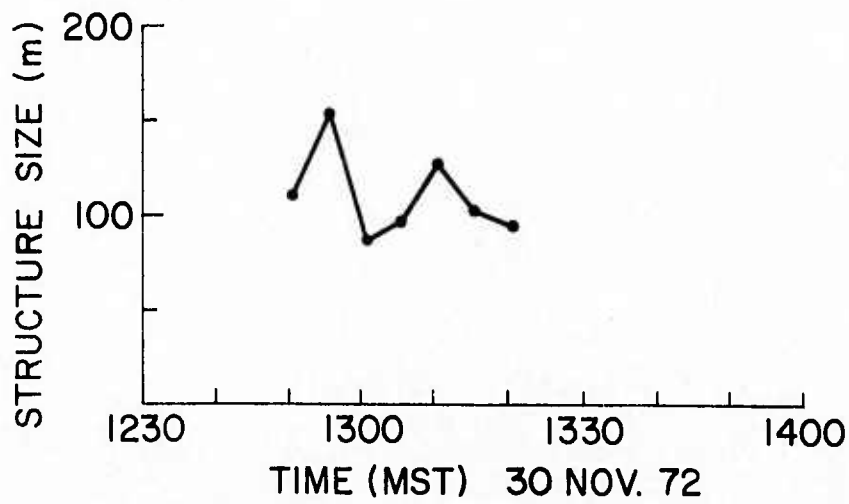
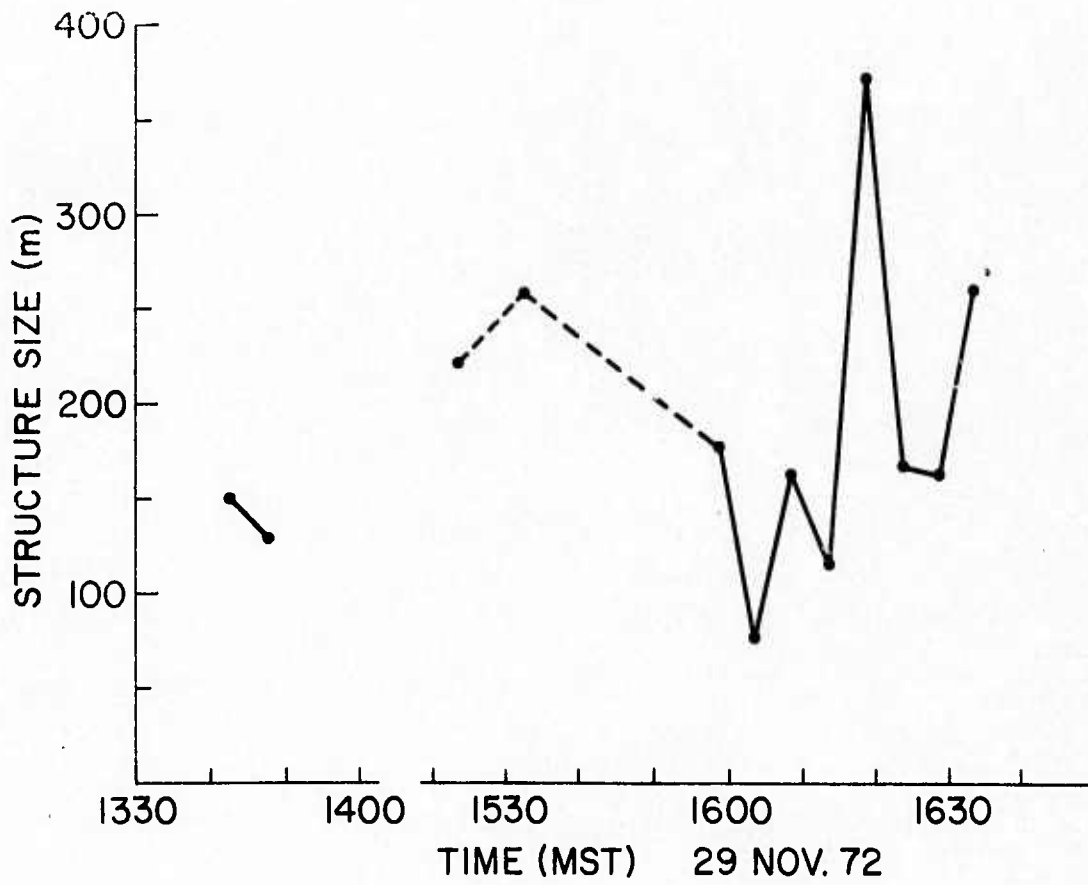


Figure 2.4 Structure size for Prairie Smoke IV (U)

SECRET

SECRET

These data were derived from cross correlations between the two pairs of antennas calculated as a function of time shift. The velocity is deduced from the ratio of the antenna spacings to the time shift for peak correlation. The time shift and east-west velocity are shown on Figure 2.3; velocity results are found comparable to those of Prairie Smoke I.

(S) The structure sizes shown in Figure 2.4 were calculated by multiplying the velocity of Figure 2.3 by the value of time shift for which the auto-correlation function dropped to a value of 0.37 ($1/e$). Assuming that the observed scintillation is completely the result of drift of the scintillating irregularities across the antenna system, these structure sizes represent the spatial separation of two antennas in the east-west direction to give a cross correlation of 0.37.

(S) In Figure 2.5 these structure size results have been combined with similar data from Prairie Smoke II, derived by manual digitization of chart records, to give an overall picture of the relative frequency of occurrence of various sizes of structure. Figure 2.6 gives a similar histogram for the magnitude of the east-west velocity.

SECRET

SECRET

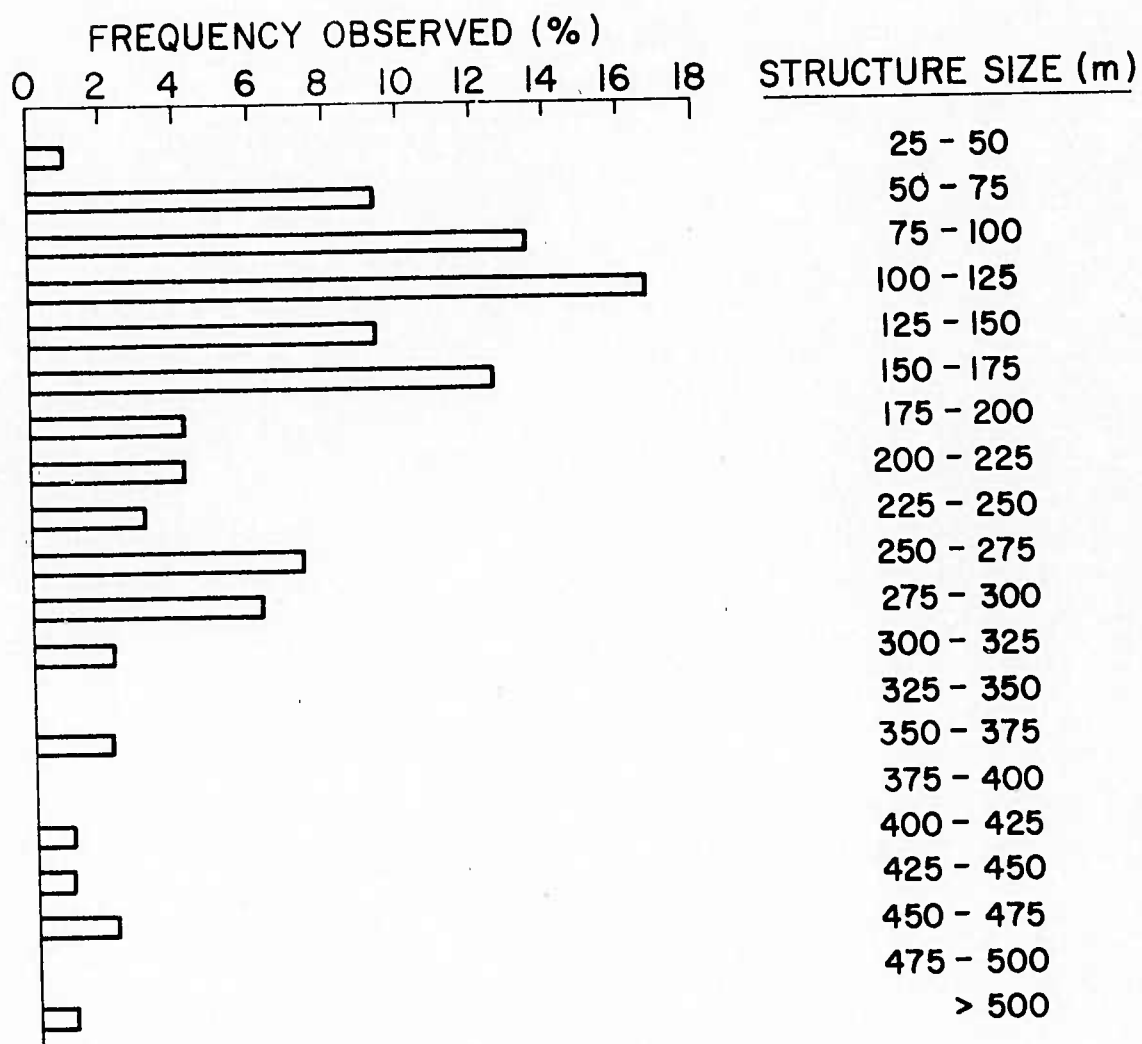


Figure 2.5 Structure size distribution for Prairie Smoke II and IV (U)

SECRET

SECRET

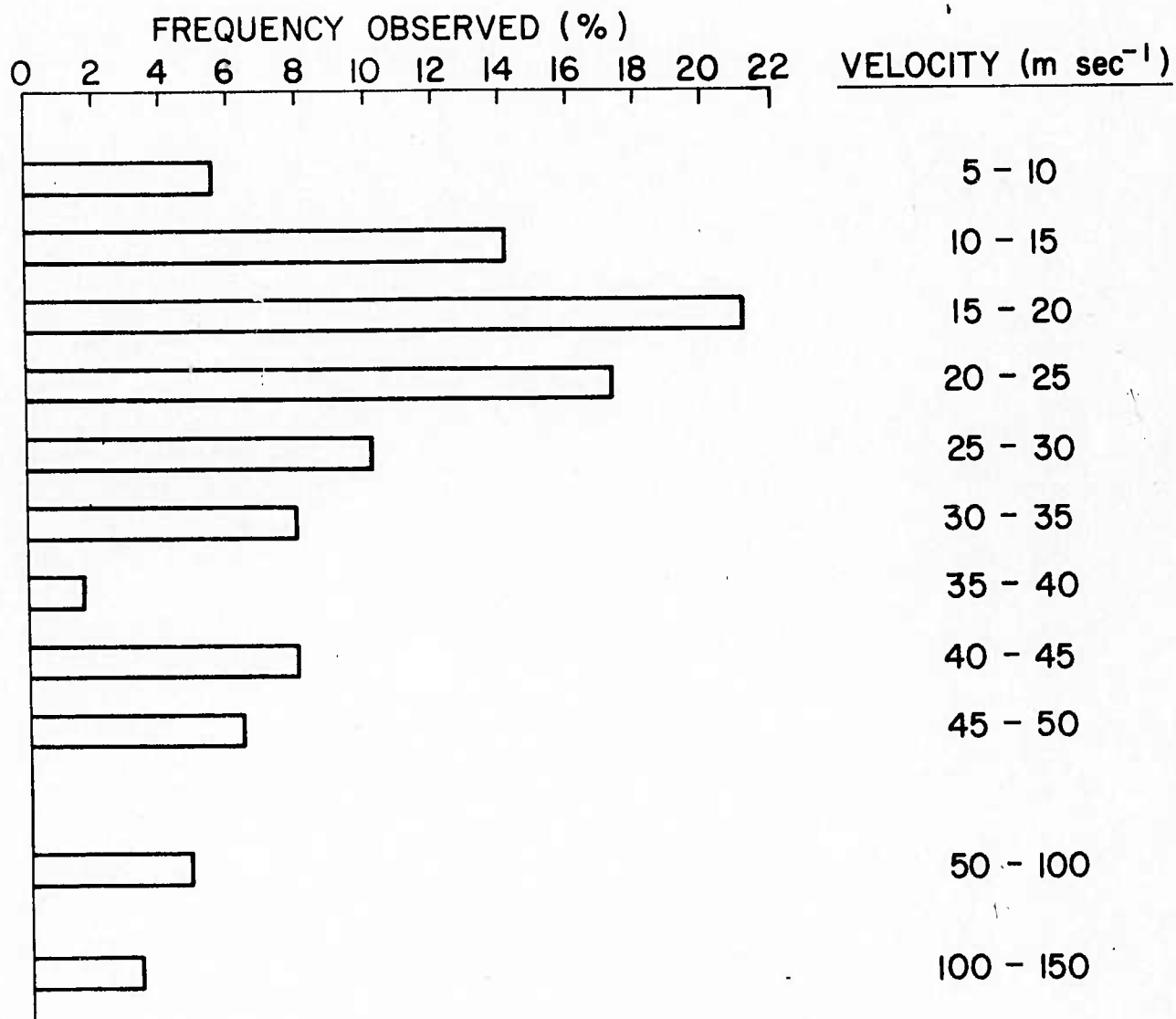


Figure 2.6 Velocity distribution for Prairie Smoke II and IV (U)

SECRET

SECRET

3. YIELD STUDIES BASED ON GEOSTATIONARY SATELLITE TRANSMISSIONS (U)

3.1 Introduction (U)

(S) The scintillation of geostationary satellite transmissions through the heated region may be used as a measure of yield. Scintillation data from Prairie Smoke II and IV were studied. The satellite scintillation data from April and May, 1972 (Prairie Smoke II) is tabulated in Table 3.1 along with the true height of reflection of the modifier signal, the value of foF2, and the frequency of the Platteville transmitter (available from the transmitter log). Also available as a yield study is a section of data from Prairie Smoke IV in which the transmitter power was varied while the value of foF2 was constant.

3.2 Data analysis (U)

(S) The scintillation index data from Prairie Smoke II is shown in Table 3.1. These data were partially taken from a previous report (Bowhill, et al., 1972a) and partially from the Prairie Smoke II transmitter log. Various parametric relationships were studied by generating a number of scatter plots from these data. A scatter plot of scintillation index versus power was prepared. One of the obvious trends in this plot is that the nighttime indices are about five times the daytime indices. This was probably caused by the line of sight passing nearer to the center of the heated region at night, when the true height level is greater. Also, group averaging implies a positive correlation of scintillation index with power as shown below:

Power	Scintillation index
1.35 MW	2.4 %
1.70 MW	3.0 %

(S) A scatter plot of scintillation index versus time of day was also prepared from the data in Table 3.1. This plot is shown in Figure 3.1. The ratio $f_H/F2$ as a percentage is shown parametrically on this plot. The data display

SECRET

SECRET

Table 3.1

Scintillation index and transmitter parameters for Prairie Smoke II (U)

Date and Time (MST)	Scintillation Index %	Transmitter		True Height (km)
		Power (MW)	$f_H/foF2$	
24 APR 1972				
1115	< 1.0	1.23	.95	240
1215	< 1.0	1.33	.95	240
1315	4.3	0.87	.89	238
1415	2.7	1.50	.87	243
1515	2.2	1.32	.88	238
1616	< 1.0	1.33	.88	240
25 APR 1972				
0615	< 1.0	1.31	.86	?
0715	3.3	1.3	.97	260
0815	4.5	.64	.96	230
0915	5.6	1.41	.87	223
1015	< 1.0	1.4	.81	208
1115	< 1.0	1.4	.97	?
4 MAY 1972				
0915	3.3	1.37	.99	235
1015	2.2	1.9	.99	235
1115	3.6	1.9	.98	253
1215	< 1.0	1.86	.81	245
1315	1.7	1.9	.76	220
1415	2.5	1.7	.78	OFF
1515	< 1.0	OFF	OFF	OFF
1615	2.8	1.87	.75	216
1715	4.8	1.65	.93	251
1815	9.6	1.64	.93	260
1915	5.7	1.64	.93	260
2015	12.0	1.56	1.00	260
2115	10.0	1.65	1.02	260
5 MAY 1972				
1115	< 1.0	1.8	.85	195
1215	3.4	1.9	≈ .83	209
1315	< 1.0	0.98	.90	209
1415	3.3	1.71	.93	209
1515	2.9	1.71	.93	209
1615	7.5	1.85	.83	233

SECRET

SECRET

Table 3.1 (Continued)

Date and Time (MST)	Scintillation Index %	Power (MW)	Transmitter $f_H/foF2$	True Height (km)	
9 MAY 1972					
0615	2.4	1.57	.99	220	
0715	1.2	1.57	1.02	220	
0815	3.2	1.57	.92	225	
0915	2.5	.88	1.00	238	
1015	4.0	.87 VAR	.87	246	
1115	2.6	1.66	.92	252	
1215	3.1	1.66	.98	257	
1315	3.9	1.66 P?	.92	262 ?	
1415	< 1.0	1.66 P?	.89	270 ?	
10 MAY 1972					
1715	< 1.0	1.55	.86	211	
1815	4.1	1.08	.87	211	
1915	4.4	1.5 ?	.95 ?	↑	Power
2015	5.3	1.65	.97	200 ?	Failure
2115	25.5	1.65	.96	↓	
11 MAY 1972					
1615	3.5	1.66	.88	247	
1715	2.9	1.66	.82	238	
1815	4.9	1.66	.79	239	
1915	< 1.0	.9 ?	.81	239	
2015	5.7	1.48	.74	239	
2115	13.7	.9 ?	1.04	230 ?	
12 MAY 1972					
1115	< 1.0	1.78	.93	239	
1215	< 1.0	1.8	.97	252	
1315	< 1.0	1.8	.88	227	
1415	< 1.0	1.8	.74	196	

SECRET

SECRET

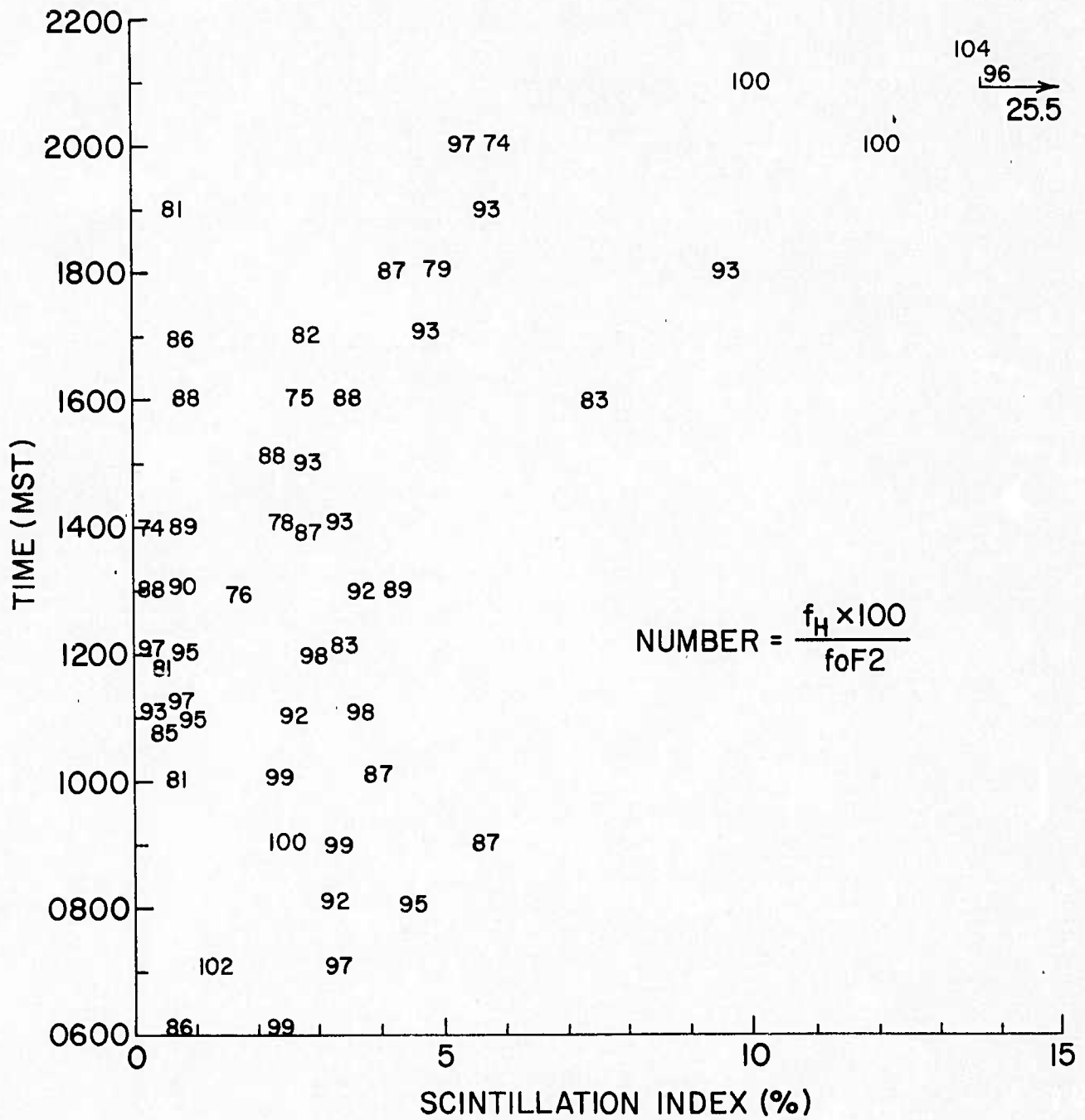


Figure 3.1 Scatter plot of scintillation index versus time (U)

SECRET

SECRET

a clear diurnal pattern in which a minimum in the typical scintillation index of less than 3% is seen near local noon, and an increase to above 10% is seen toward late evening. If all the data below one percent are ignored (no observed scintillation), the diurnal pattern is particularly clear.

(S) A yield study was also made on some of the geostationary satellite data from Prairie Smoke IV. Figure 3.2 is a scatter plot taken from a section of data approximately 35 minutes long from 30 November 1972. The transmitter power was varied in several steps during this time. It was 3 dB below full power for the first 12 minutes, then 6 dB below for the next 13 minutes, and finally at full power for the last 10 minutes. The scintillation index was calculated over one-minute intervals during this time. A scatter plot of the results is shown in Figure 3.2. The plot shows scintillation indices ranging from 3.5 to 19.5 % as the power is varied over the 6 dB domain. The straight line shown has been drawn through the average value for each power level. From the slope of this line, it may be shown that the scintillation index is approximately proportional to the square root of the modifier power.

SECRET

SECRET

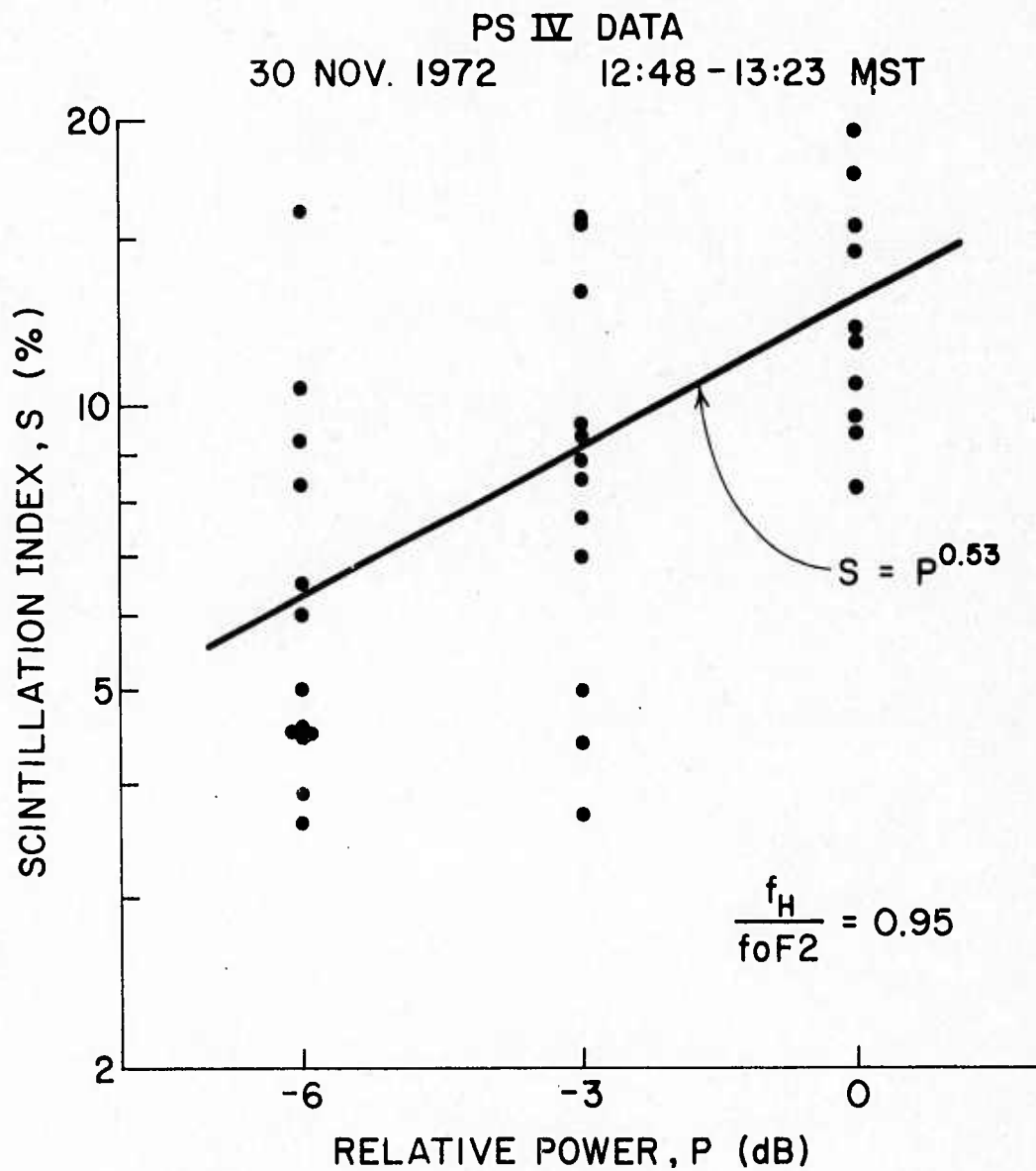


Figure 3.2 Scatter plot of scintillation index versus power (U)

SECRET

SECRET

4. CORRELATION ANALYSIS OF PRAIRIE SMOKE TRANSMISSION RESULTS (U)

4.1 Introduction (U)

(S) Auto- and cross-correlation analysis has been carried out on automatically digitized amplitude scintillation data derived from orbital satellites in Prairies Smoke Ib and III. This analysis is much more accurate than previous studies using hand-reduced data. These data are used to calculate the dip angle of artificial spread F (ASF) irregularities causing scintillation of satellite signals in Prairie Smoke Ib; and to demonstrate the presence of small-scale structure in the ASF of Prairie Smoke III. These analyses are described in Sections 4.2 and 4.3, respectively.

4.2 Irregularity orientation in Prairie Smoke Ib (U)

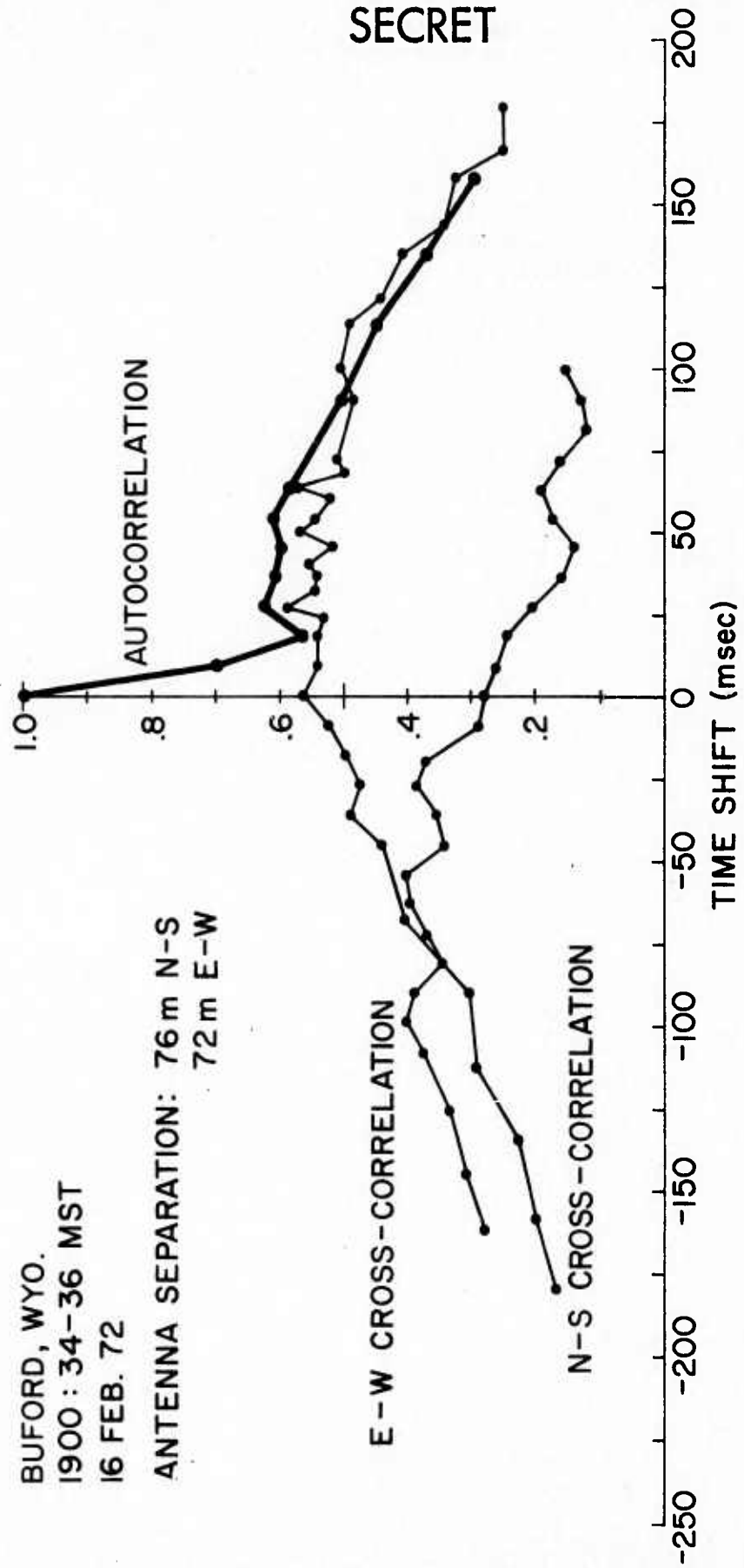
(S) In a previous paper (Bowhill, et al., 1972a) an analysis was presented of the orientation observed for the line of maximums of the scintillations of the signal from an orbital satellite on 16 February 1972 in Prairie Smoke Ib. This analysis was based on visual inspection of chart records of signal amplitude, and showed that the orientation of the line of maximums with satellite position was more or less as would be expected if the irregularities causing the scintillations were field-aligned.

(S) Digital correlation analysis has now been carried out for these data. The analog data, in the form of audio signals centered on 2-3 kHz frequency, were passed through a tracking filter and a detector with 1 msec time constant. They were then digitized at a 1 kHz rate and a correlation analysis performed for the three signals from antennas spaced in a north-south and east-west direction using a PDP-8e computer. Typical auto- and cross correlations are shown on Figures 4.1 and 4.2 and for two times during the pass of a US Navy Navigational satellite over Buford, Wyoming on February 16, 1972, based on amplitude measurements at 150 MHz. The rapid decrease of autocorrelation

SECRET

BUFORD, WYO.
1900 : 34-36 MST
16 FEB. 72

ANTENNA SEPARATION: 76 m N-S
72 m E-W



SECRET

SECRET

Figure 4.1 Auto- and cross correlations early in pass (U)

SECRET

BUFORD, WYO.
1901:16-18 MST
16 FEB. 72

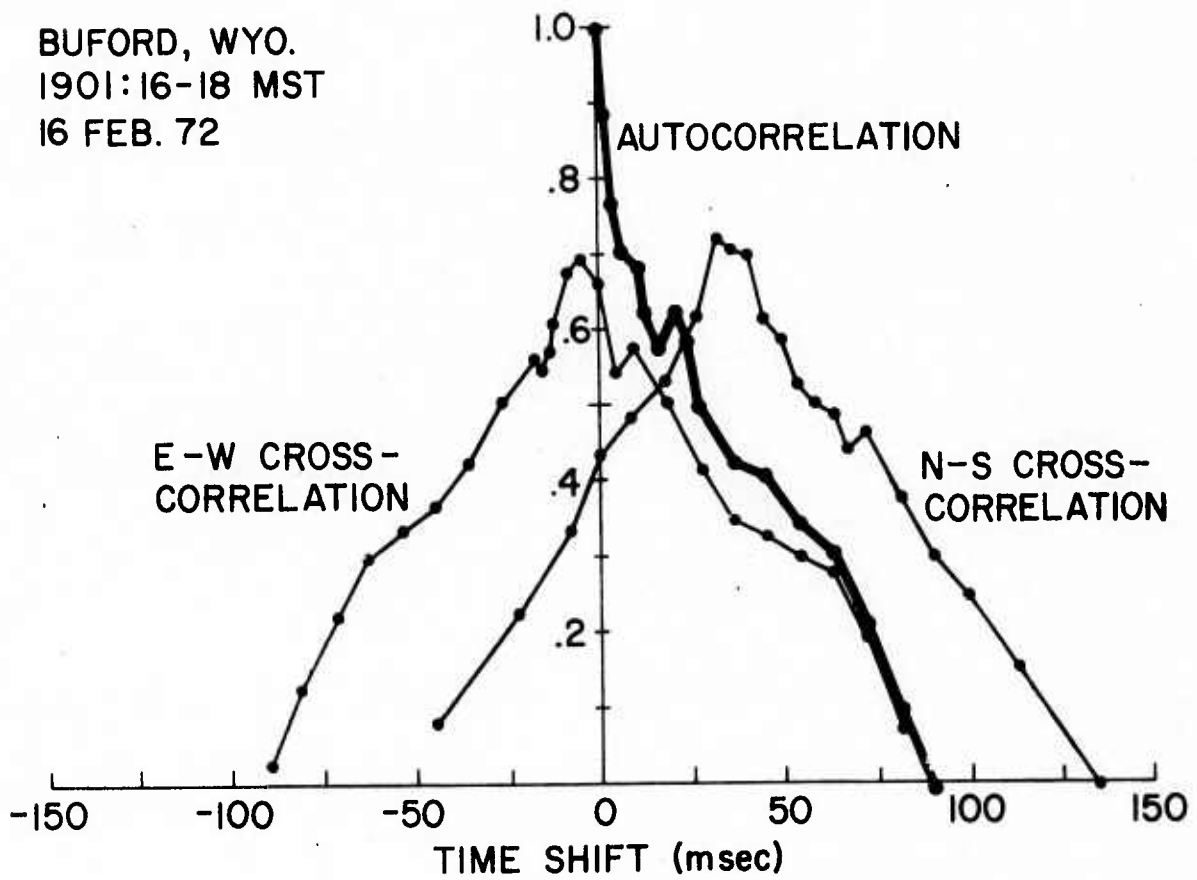


Figure 4.2 Auto- and cross correlation late in pass (U)

SECRET

SECRET

from 1 to .6 in Figure 4.1 and to about .7 in Figure 4.2 simply represents the contribution of receiver noise to the total decorrelation. Since the north-south cross correlation reaches a maximum value very close to the signal auto-correlation at zero time shift, it is clear that the scintillations are due to highly elongated irregularities. By observing the time shifts of the cross correlations and relating them to the satellite velocity, the height of the irregularities can be determined. A series of these time shift measurements is illustrated on Figure 4.3. The orientation of the major axis of the scintillation irregularities can be calculated from these time shifts, and is illustrated on Figure 4.4. Also shown on Figure 4.4 is the variation of axis orientation with time that would have occurred had the irregularities been oriented in the magnetic meridian with magnetic dips of 61.2, 68.2 and 75.2 deg. Clearly, there are systematic departures from the normal magnetic dip of 68.2 deg which is thought to be appropriate for Platteville.

(S) It is possible to calculate the dip angle of the irregularities that would produce the observed axis orientation. This is plotted in Figure 4.5 as a function of time during the pass. The wide variations in the angle suggest the plot of Figure 4.6 as a function of the height of the irregularities deduced from the observed time shifts, and a systematic relationship is seen to be present. Since the magnetic dip varies throughout the satellite pass, these results have been compared with a magnetic field model in which the dip over Platteville is 68.2 deg, and the departure is shown in Figure 4.7. This result suggests that the ASF irregularities are banana-shaped, being oriented approximately parallel to the magnetic field at the reflection height of the heater (about 230 km), but closer to the vertical at higher altitudes and closer to the horizontal at lower altitudes. The reason for this may be connected with the variation of Pedersen conductivity with altitude, combined with the effects of ion drag from the motion of the thermosphere.

SECRET

SECRET

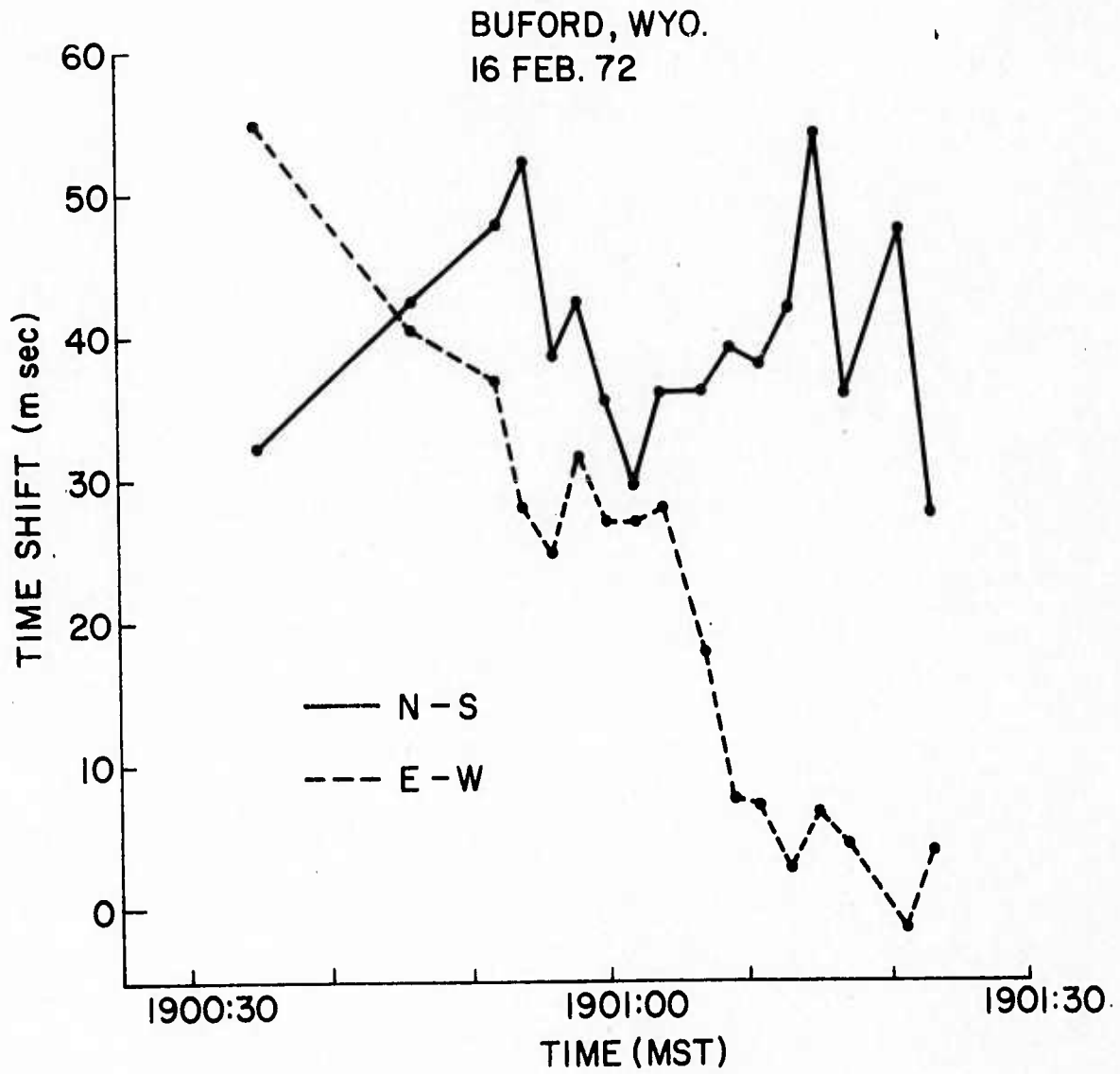


Figure 4.3 North-south and east-west time shifts (U)

SECRET

SECRET

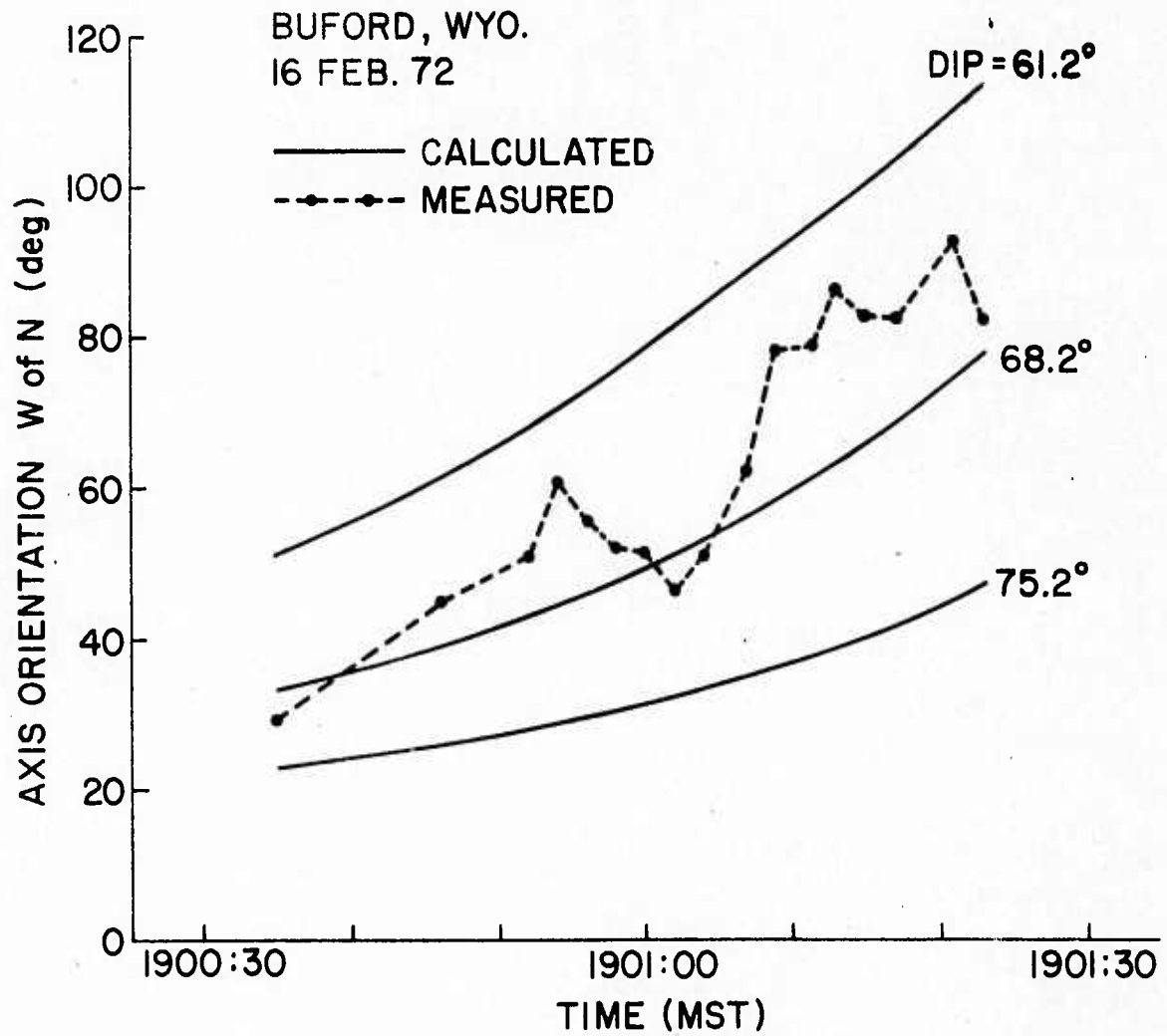


Figure 4.4 Scintillation axis orientation versus time compared with model (U)

SECRET

SECRET

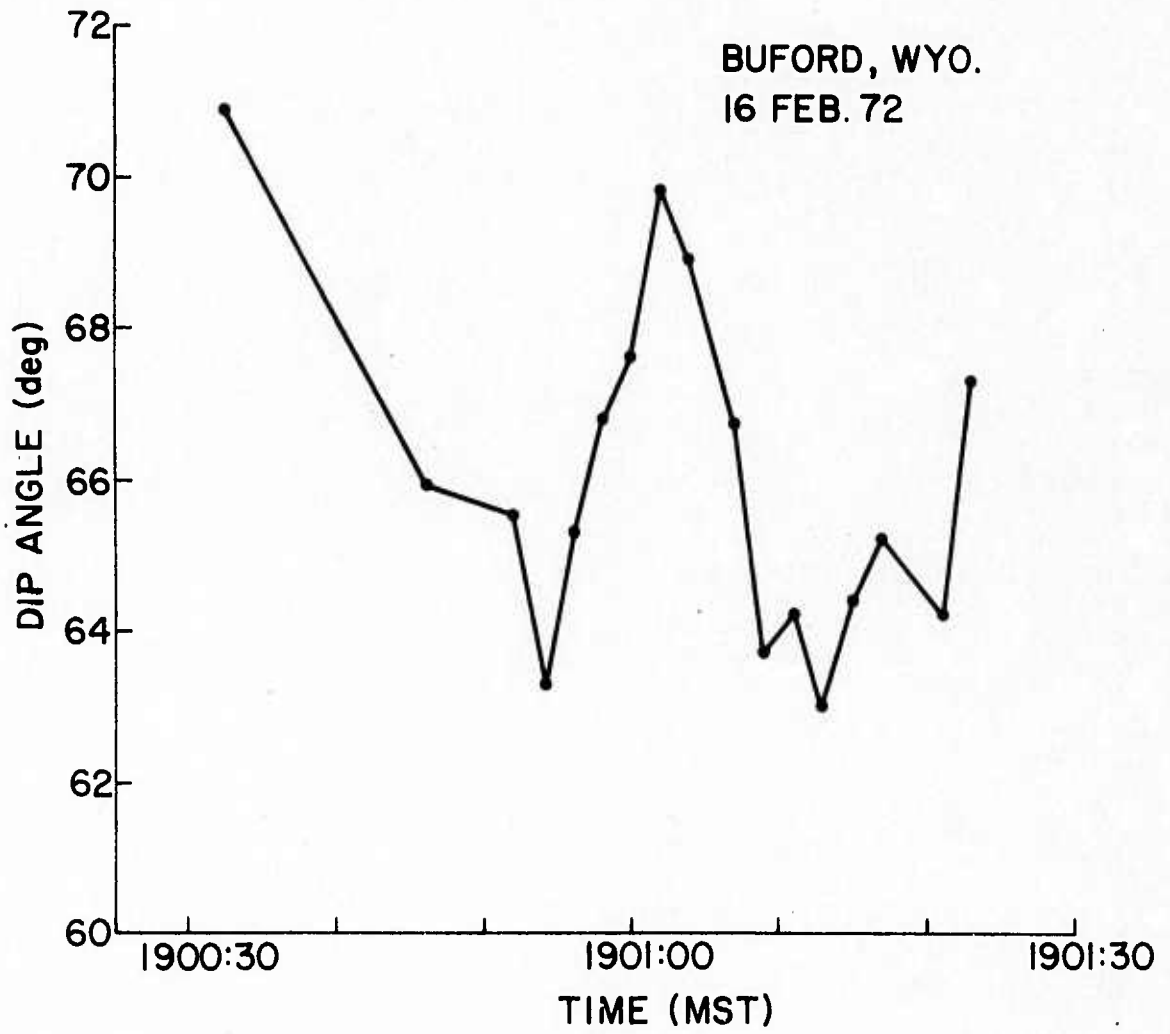


Figure 4.5 Apparent dip angle versus time (U)

SECRET

SECRET

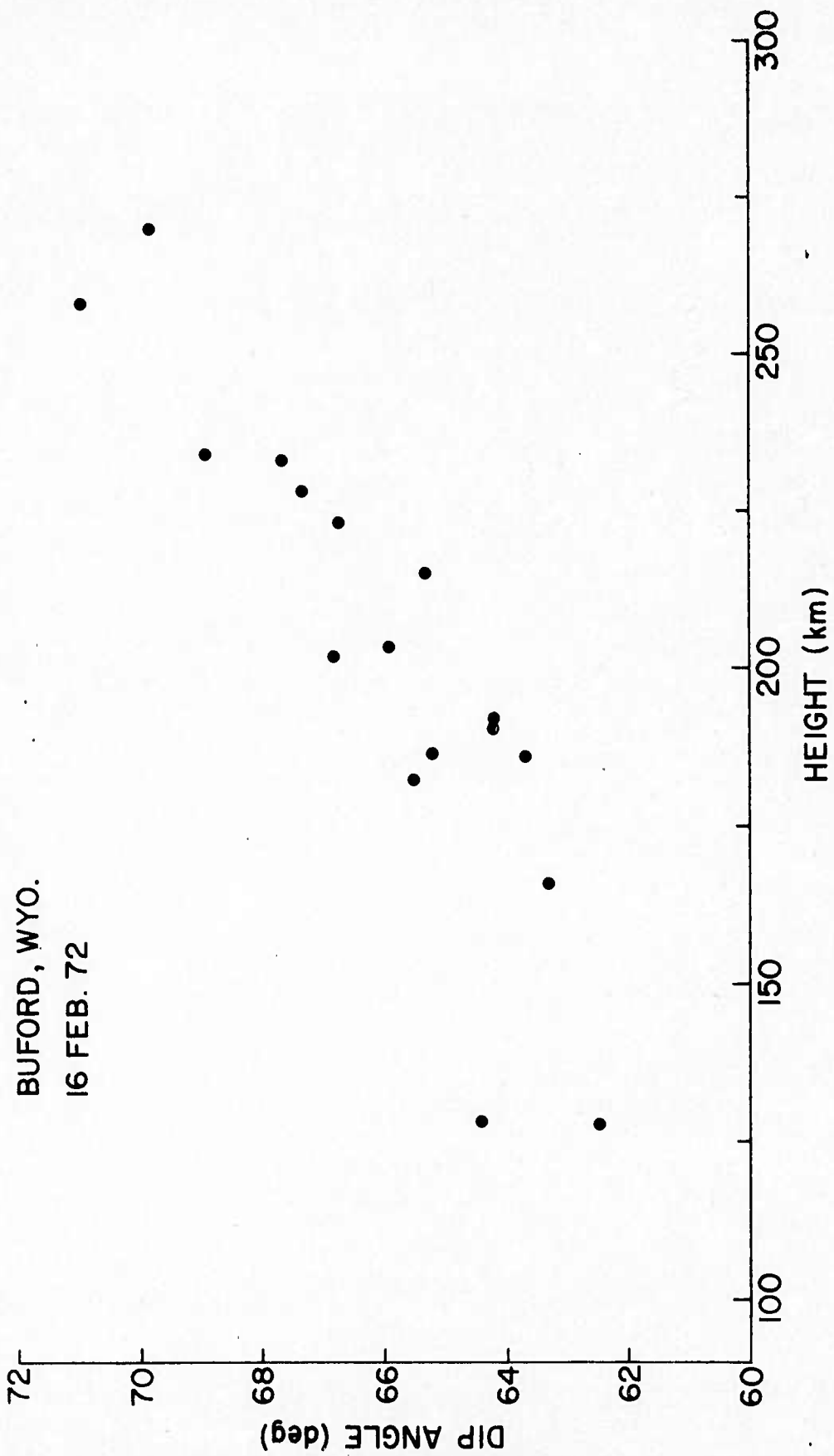
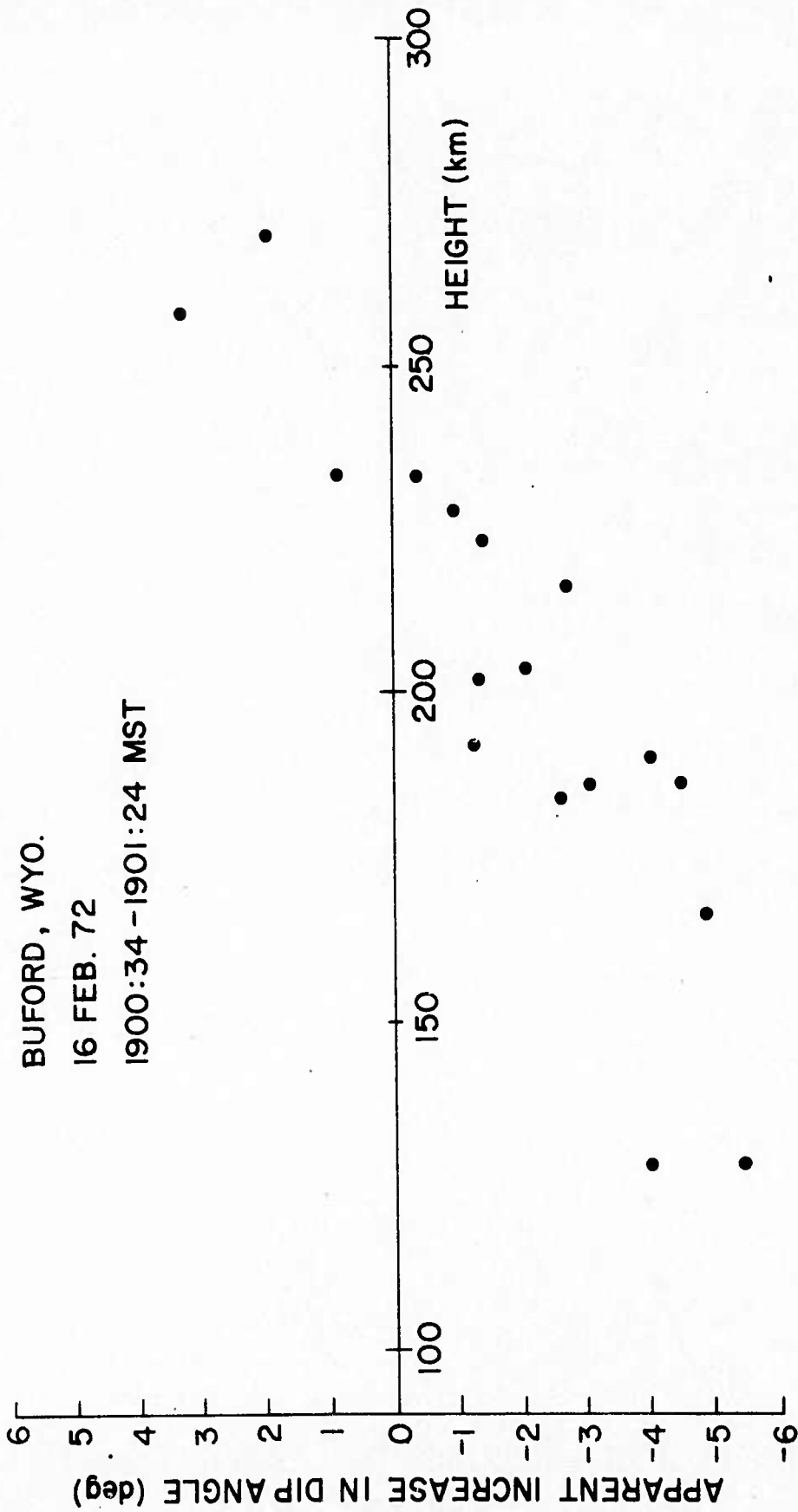


Figure 4.6 Apparent dip angle versus observed height (U)

SECRET

SECRET



SECRET

Figure 4.7 Apparent increase in dip angle versus height (U)

SECRET

4.3 Irregularity characteristics in Prairie Smoke III (U)

(S) In a previous paper (Bowhill, et al., 1972b) it was suggested that fine structure less than 10 m in size was visible on cross-correlation records from spaced antennas, using signals at 150 MHz from orbiting satellites. This analysis has been continued for other satellite passes using the digitization scheme described in the previous section. The results are presented here for an interesting pass in Prairie Smoke III.

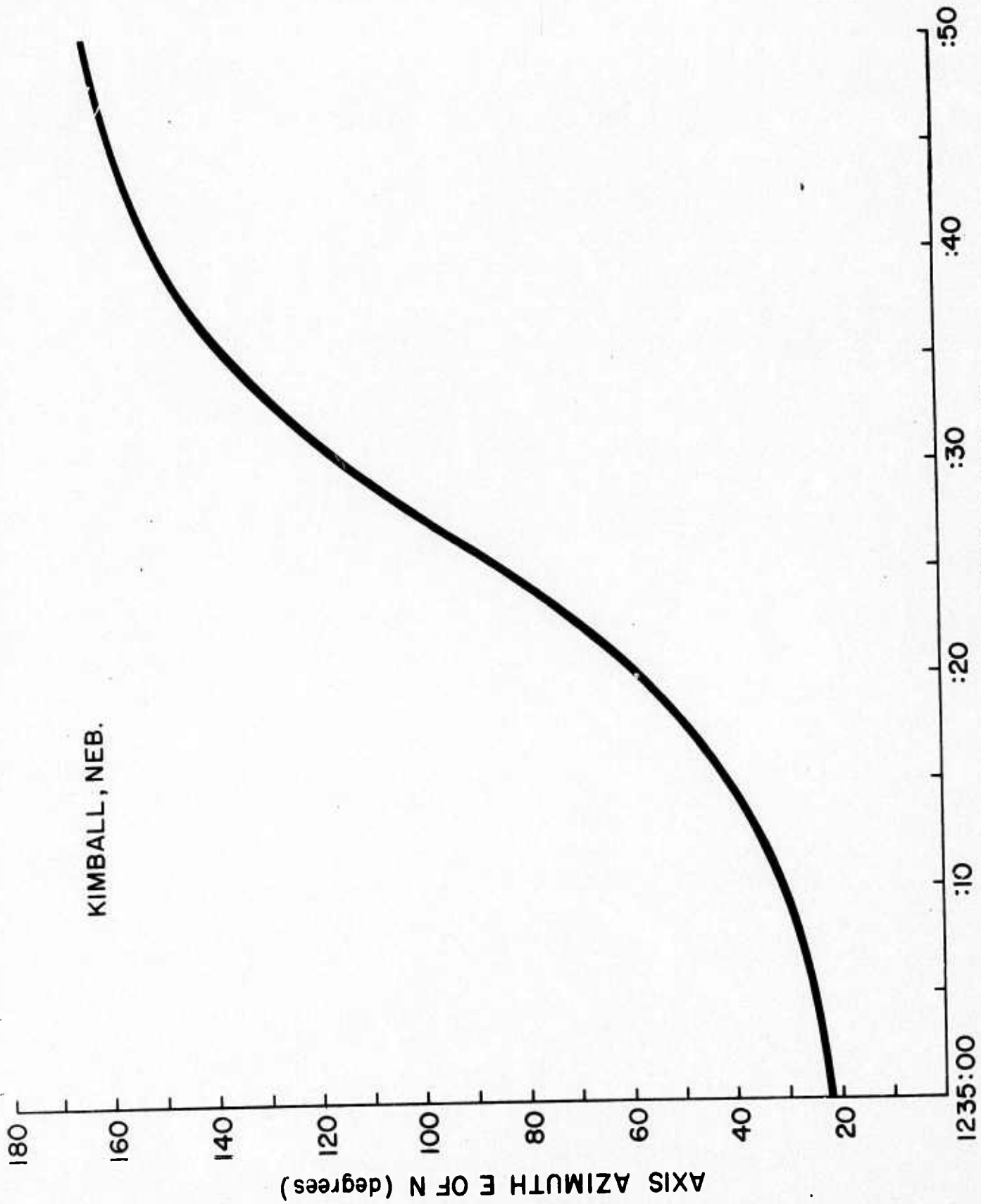
(S) During the period 1235:00 to 1235:50 MST on September 8, 1972, a US Navy Navigational pass was observed at Kimball, Nebraska. Since it passed close to the upfield direction, the magnetic field projected along the line of sight rotated about 140 deg as indicated in Figure 4.8. A typical cross correlation for a 2-second period during this time is illustrated in Figure 4.9, showing the characteristic peaked shape due to fine structure. Figure 4.10 which is averaged over four successive 2-second samples, shows the peaked cross-correlation function even more clearly.

(S) Based on the shape of the cross-correlation function, structure sizes can be deduced from the large- and small-scale structures. Neglecting the effects of field alignment, these are found to vary as shown in Figure 4.11 throughout the pass. When field alignment is taken into account, the structure size shown in Figure 4.12 is found in the direction normal to the magnetic field. It is seen that the large- and small-scale structures seem to vary together by about a factor of three through the pass, their ratio remaining about 15 or 20 to 1.

(S) A further experiment (Prairie Smoke IVb) was carried out on February 22, 1973, at Hillsdale, Wyoming with X-mode heating in the disturbed region. Some signs of small-scale structure were seen in the scintillation of an orbiting satellite at 150 MHz, though the scintillations were weaker by a factor of 2 or 3 than those observed with O-mode heating, described earlier in this section.

SECRET

SECRET



TIME (MST) 8 SEP. 72

Figure 4.8 Scintillation image axis orientation (U)

SECRET

SECRET

KIMBALL, NEB.
1235:16-18 MST
8 SEP. 72

ANTENNA
SEPARATION: 76 m N-S

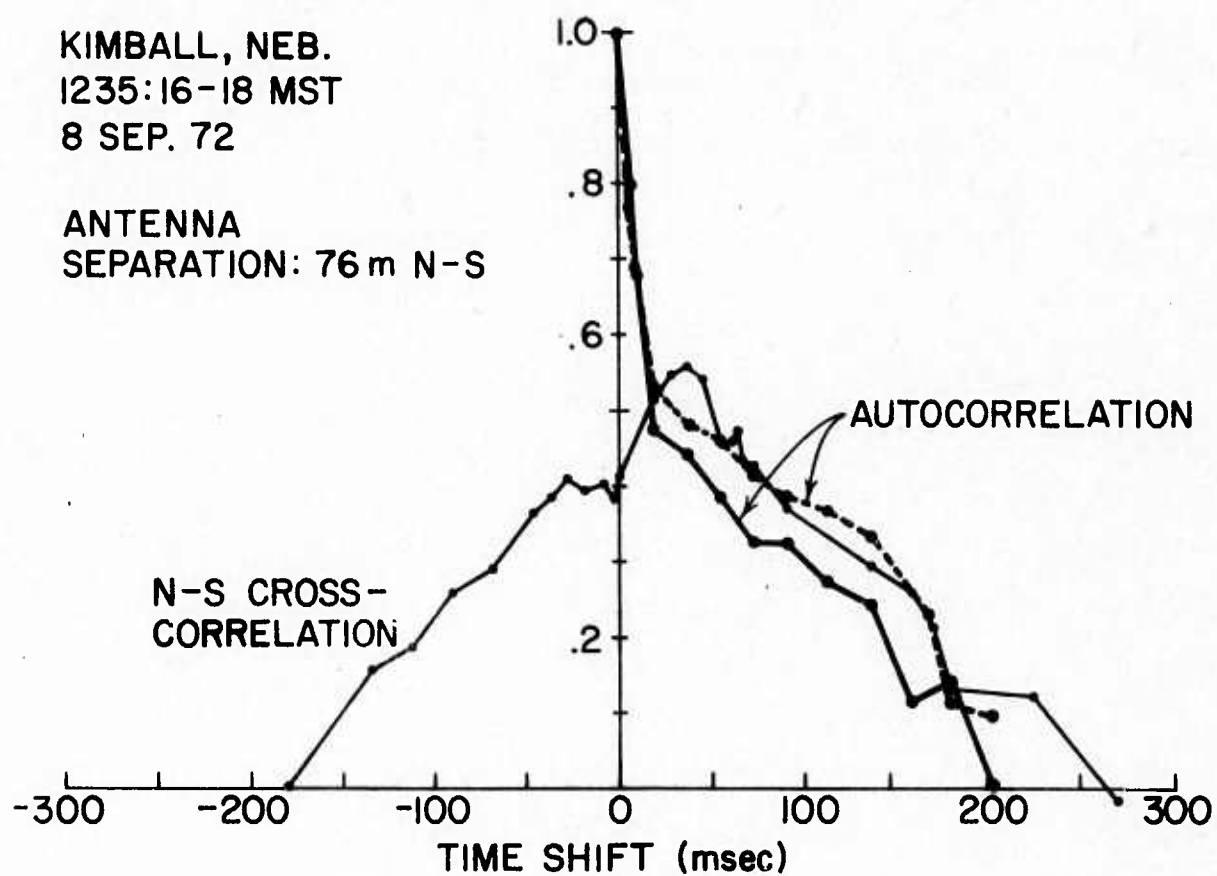


Figure 4.9 Auto- and cross correlations in Prairie Smoke III (U)

SECRET

SECRET

KIMBALL, NEB.
1235:17-25 MST
8 SEP. 72

ANTENNA
SEPARATION: 76m N-S

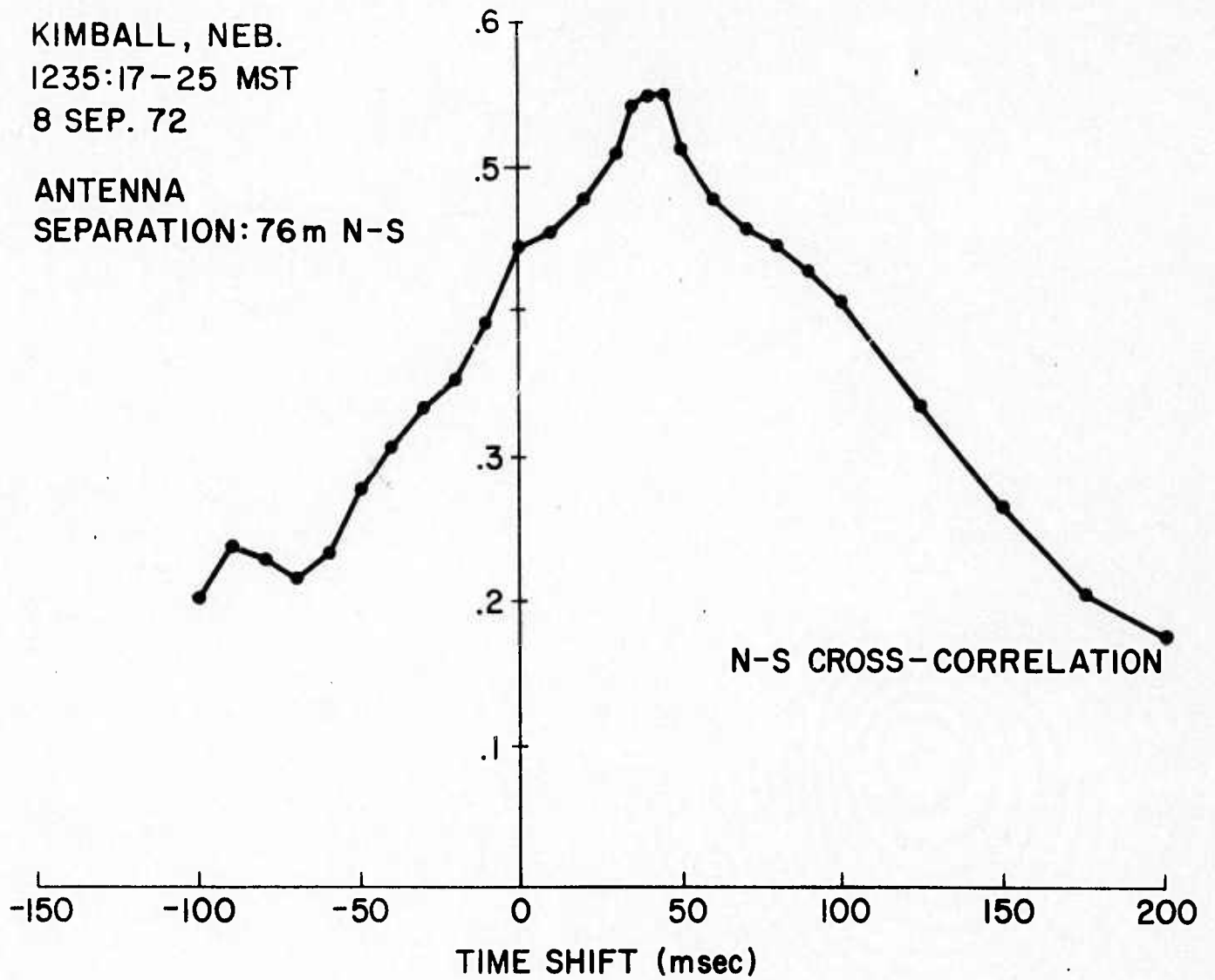
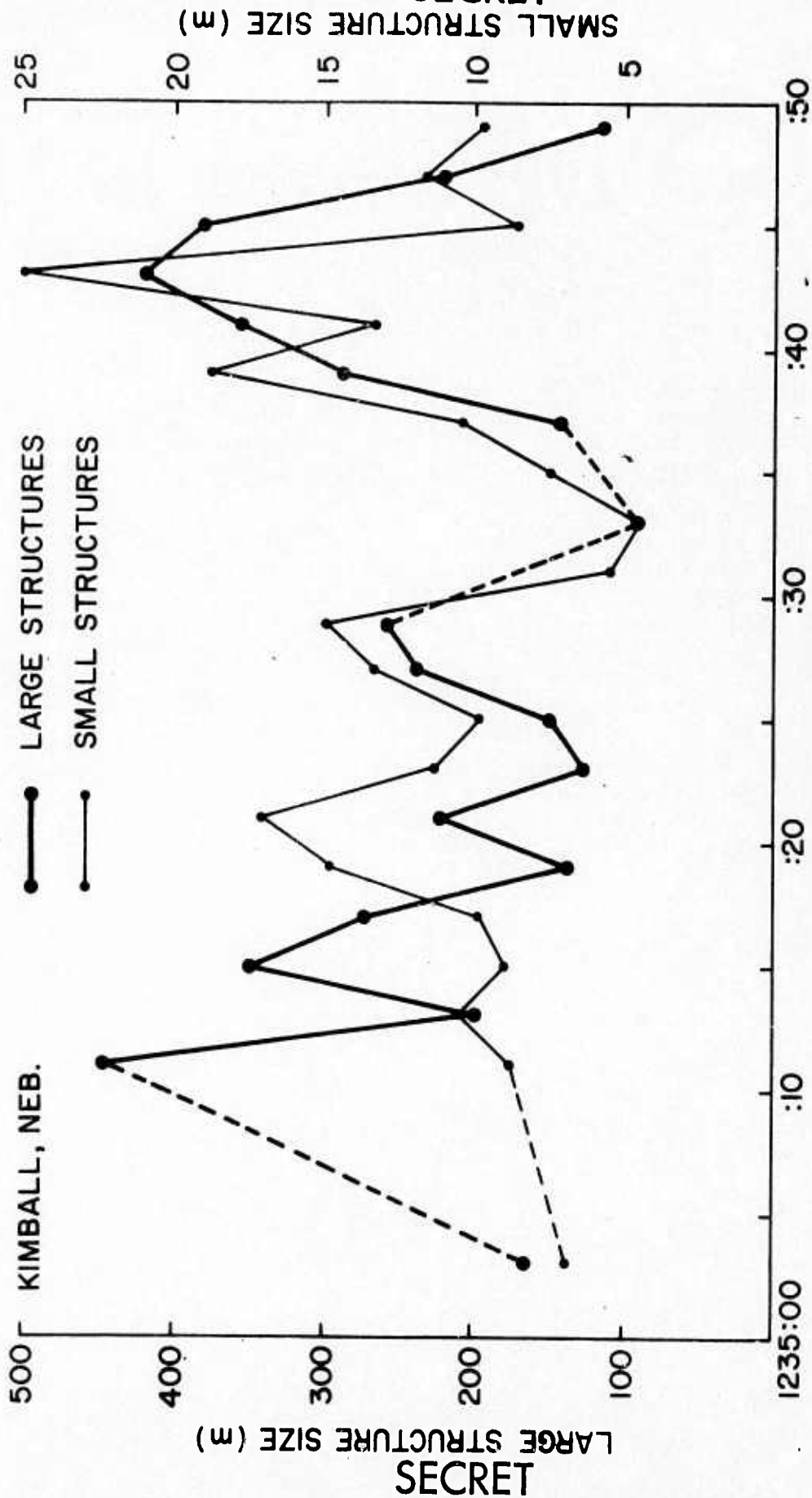


Figure 4.10 Average cross correlation for Prairie Smoke III (U)

SECRET

SECRET



TIME (MST) 8 SEP. 72

Figure 4.11 Structure sizes neglecting field alignment (U)

SECRET

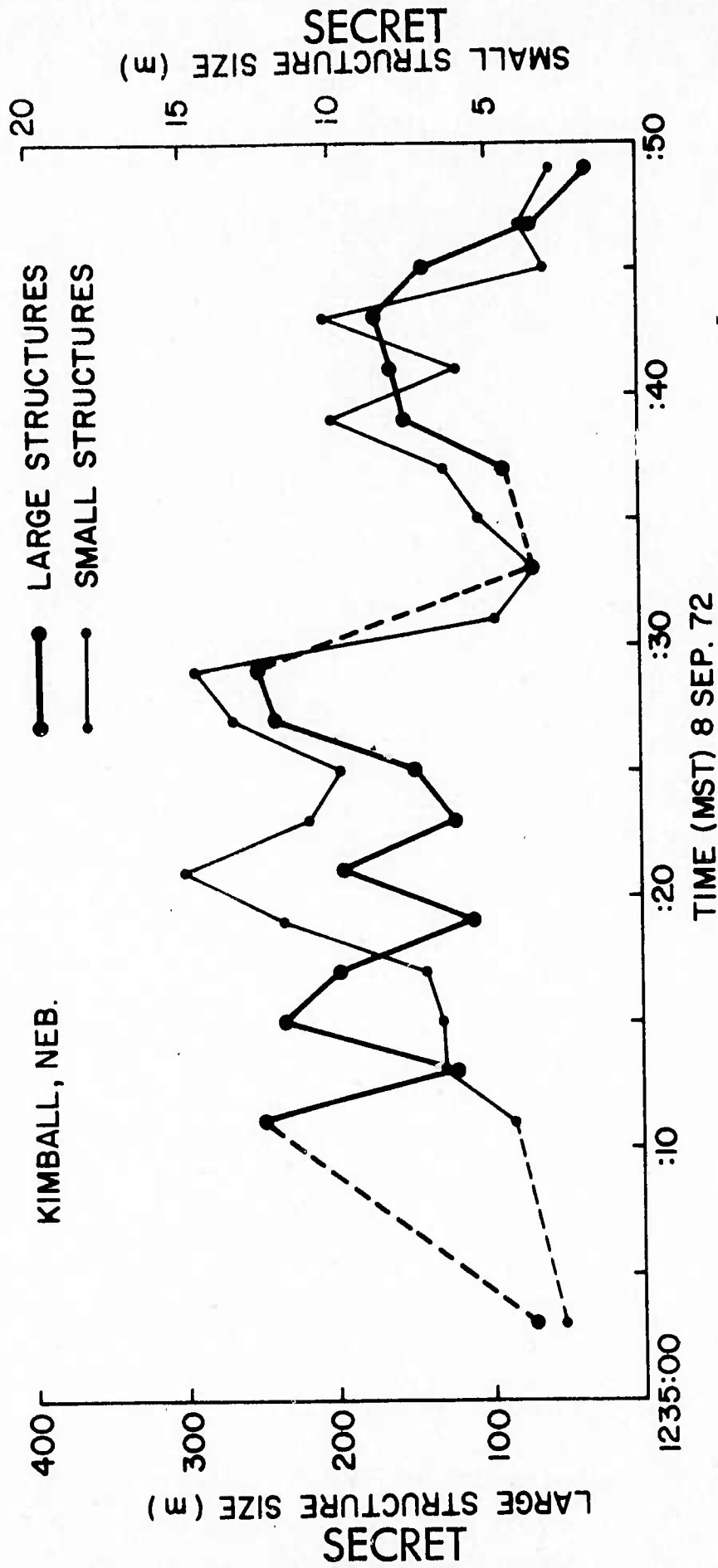


Figure 4.12 Structure sizes assuming field alignment (U)

SECRET

5. MODEL FOR SCINTILLATION AND SPREAD F (U)

5.1 Description of artificial field-aligned irregularities (U)

(S) The large-scale field-aligned irregularities in ionization produced in the F layer by intense RF heating have been described as artificial spread F (ASF). To clarify the reason for this description, the properties of naturally-occurring spread F (NSF) are briefly described, as are the characteristic differences between NSF and ASF. The properties of ASF are then combined into a single rational model suitable for systems-analysis purposes.

5.2 Natural spread F (U)

(S) NSF derives its name from the appearance produced on a sweep-frequency ionogram by irregularities in F-region ionization. These have been investigated extensively, and have indeed been the subject of a conference (Newman, 1966). While NSF has been classified into several distinct kinds, its mechanism of origin remains a mystery, as far as the temperate-latitude manifestations are concerned. Certain facts, on the other hand, seem fairly clear:

1. NSF is primarily a nighttime phenomenon, occurring to various degrees on perhaps 10 - 20 percent of nights at a typical mid-latitude station.
2. NSF tends to occur in patches several thousand kilometers in diameter, which seem to originate around magnetic latitude 60 deg and spread to lower latitudes.
3. The irregularities producing NSF are in the form of randomly arranged ellipsoidal enhancements or depletions of ionization, the principal axes of the ellipsoids being parallel to the local magnetic field direction, and the ellipsoids being centered approximately on the F-region peak. In a horizontal direction, the electron-density profile has a random fluctuation with distance, the correlation

SECRET

SECRET

function of the variation having an e-folding distance of about 1 km.

4. Parallel to the magnetic field, the enhancements or depletions of ionization continue through the F-region peak, and the fractional fluctuation in electron density seems to be approximately independent of altitude.
5. The spreading of ionosonde traces can be explained as due to trapping of obliquely incident signals in field-aligned ducts produced by the ionization depletions, causing the wave to be trapped and reflected at a range exceeding the normal range. This ducting is visible both from the bottom and topside (from sweep-frequency sounders on satellites).

5.3 Artificial spread F (U)

(S) The leading features of ASF may be compared with NSF as follows (using the same numbering as in Section 5.2):

1. ASF occurs on every occasion when ordinary-mode heating is used at a frequency slightly less than f_oF_2 . However, it appears to be more severe at night for the same heating power.
2. ASF occurs in an approximately circular region with radius about 50 km centered slightly north of the heater transmitter, with an onset and decay time of about a minute relative to the time of heating. The intensity of the irregularities is somewhat nonuniform in the horizontal direction, perhaps due to variations in the intensity of heating produced by gross horizontal inhomogeneities in the F layer.
3. As with NSF, the irregularities are field aligned with maximum intensity in the F-region peak. However, the e-folding distance of the horizontal correlation function of the structures is about one-tenth of the natural scale; namely, about 100 m. The ASF irregularities move horizontally with a few tens of m/s, apparently corresponding

SECRET

SECRET

to horizontal motions of the entire F layer.

4. As with NSF, the ASF irregularities continue all through the F layer from 200 to about 450 km altitude, their intensity being approximately proportional to the ambient electron density.

5.4 Analytical model for ASF (U)

(S) The easiest aspect of ASF to quantify is its effect on a UHF radio signal transmitted through the ionosphere. As indicated in Section 5.2, such a signal undergoes a random phase perturbation with rms value γ , given by

$$\gamma^2 = \frac{\pi^{5/2}}{\lambda^2} \left(\frac{f_oF2}{f}\right)^4 \int_0^{h_s} D \sec i \operatorname{cosec} \psi g^2(x,y,h) \left(\frac{N}{N_m}\right)^2 dh \quad (5.1)$$

Now consider a satellite height h_s which is far above the F-layer peak; zenith angles less than about 60 deg (so that earth curvature can be neglected); and irregularity size D which is independent of altitude. Choose the coordinate system shown in Figure 5.1, x to the magnetic north, y to the magnetic east and h vertically. Take the coordinate origin at the heater transmitter, then the center of the disturbed region at 300 km height, and x_0 to the north has coordinates

$$(x_0 - (h - 300) \cot \delta, 0, h)$$

where δ is the local magnetic dip. Other than x_0 the three parameters that seem to be required to specify the general form of the spatial variation of g are the value g_0 at the center of the disturbed region; and its e-folding distances X, Y in the north-south and east-west directions. Within the region where earth curvature and magnetic field curvature may be neglected, the spatial variation of g seems to be well represented by

SECRET

SECRET

$$g^2 = g_0^2 \exp \{-[x - x_0 - (h - 300) \cot \delta]^2/X^2 - y^2/Y^2\} \quad (5.2)$$

For typical conditions correspond to ordinary-wave heating with maximum power, the following approximate values of the parameters apply:

$$\begin{aligned} g_0 &= .007 \\ x_0 &= 30 \text{ km} \\ X &= Y = 50 \text{ km} \end{aligned}$$

Inserting from equation (5.2) into (5.1), with the approximations listed above, we obtain

$$\begin{aligned} \gamma^2 = \frac{\pi^{5/2}}{2} \left(\frac{foF2}{f}\right)^4 D \sec i \operatorname{cosec} \psi g_0^2 \int_0^\infty \left(\frac{N}{N_m}\right)^2 \exp \{-[x-x_0 + (h-300) \cot \delta]^2/X^2 \\ -y^2/Y^2\} dh \end{aligned} \quad (5.3)$$

In this equation, of course, the values of X and Y are parametrically determined as functions of h by the equation for the line of sight (which will be a straight line for the conditions of UHF propagation for which equation (5.1) applies).

(S) The integral in equation (5.3) can be conveniently evaluated once we note that most of the height valuation of the integrand is contained in the term $\left(\frac{N}{N_m}\right)^2$, and that the exponential of the integrand is nearly constant over most of the range of interest. To a good approximation, therefore, we may write

$$\begin{aligned} \gamma^2 = \frac{\pi^{5/2}}{2} \left(\frac{foF2}{f}\right)^4 D \sec i \operatorname{cosec} \psi g_0^2 \exp \{-x_m-x_0 + (h_m-300) \cot \delta\}^2/X^2 \\ -y_m^2/Y^2 \int_0^\infty \left(\frac{N}{N_m}\right)^2 dh \end{aligned} \quad (5.4)$$

SECRET

SECRET

where the integral in this equation is typically about 120 km, and x_m and y_m are the coordinates at which the line of sight intercepts the height of maximum of the layer.

(S) If we further make the approximation that the region of disturbance is circular, we can put $X = Y = R$, and equation (5.4) becomes

$$\gamma^2 = \frac{\pi^{5/2}}{\lambda^2} \left(\frac{foF2}{f}\right)^4 D \sec i \operatorname{cosec} \psi g_0^2 \exp(-r^2/R^2) \int_0^\infty \left(\frac{N}{N_m}\right)^2 dh \quad (5.5)$$

where r is the horizontal distance between a point where the line of sight intercepts the height of maximum of the layer, and a point at the same height on the field line that passes a distance x_0 north of the heater transmitter at an altitude of 300 km.

(S) The variation of g_0^2 with yield is well represented by a proportionality to heater power; there is some evidence that the value of g_0 at night is approximately twice that during the day, though focussing effects produce variations in x_0 that tend to make this effect less definite.

SECRET

SECRET

6. THE INCLUSION OF ANTENNA POWER PATTERNS IN THE SCATTERING MODEL (U)

6.1 Introduction (U)

(S) In any attempt at determining the yield of a heater transmitter, the antenna pattern should be included. In this study, a fairly simple yield model was combined with a fairly complete antenna polar diagram computation. The results include a revealing study of the antenna polar diagram itself under variations in frequency, tilt angle, and the antenna configuration. Also, the radar cross section as a function of slant range was studied and found to be quite sensitive to the antenna polar diagram and tilt angle. The results, especially the effects of the sidelobes, have proven to be very interesting.

(S) Finally, it is shown that beam tilting may often be used to increase the relative cross section if the reflection point and heating height are mismatched at overhead Platteville.

(S) The antenna polar diagram was studied using a computer program which computed the relative power per steradian in a requested number of directions. Each element of the antenna is a crossed dipole above a conducting ground screen. The HF array elements are 30 feet above the ground, and the MF array elements are 60 feet above the ground. The only approximation used was to assume the free-space pattern of the dipoles to be the same as that of a short (with respect to a wavelength) dipole. The input to the program was fairly flexible, consisting of the signal frequency as well as the position of each element and the amplitude and phase of the signal at that element. This program allows any antenna configuration to be studied, however we have confined ourselves to studying available antenna configurations (see Figure 6.1)

6.2 Antenna polar diagrams (U)

(S) A number of cases of interest were studied, and the polar diagrams are presented in Figures 6.2 through 6.8. Table 6.1 summarizes some of the parameters

SECRET

SECRET

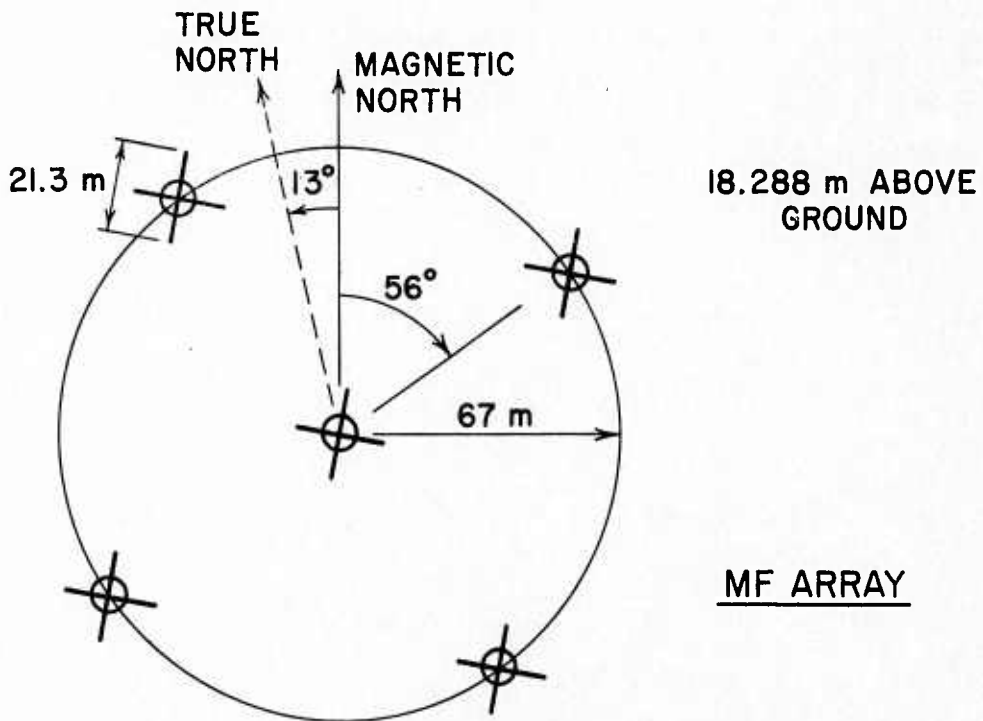
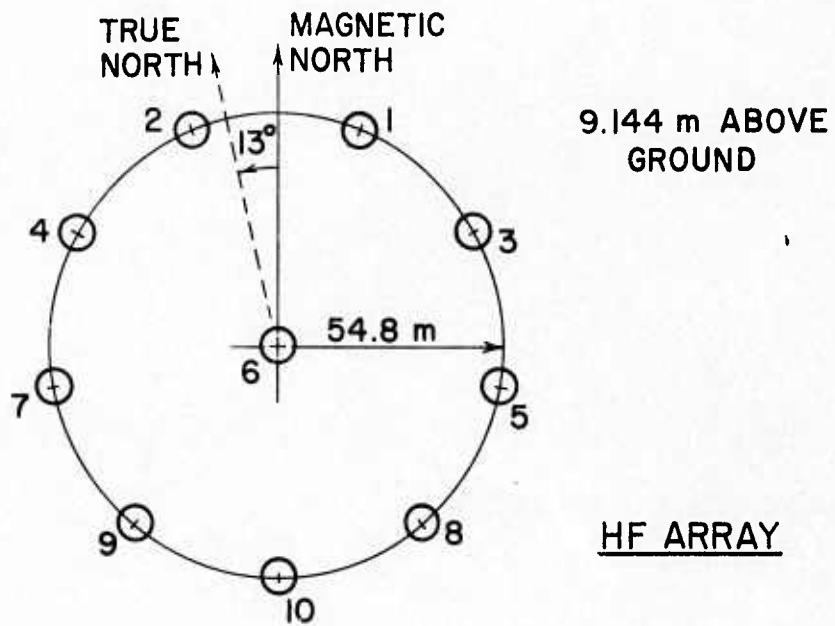


Figure 6.1 Antenna configurations available (U)

SECRET

SECRET

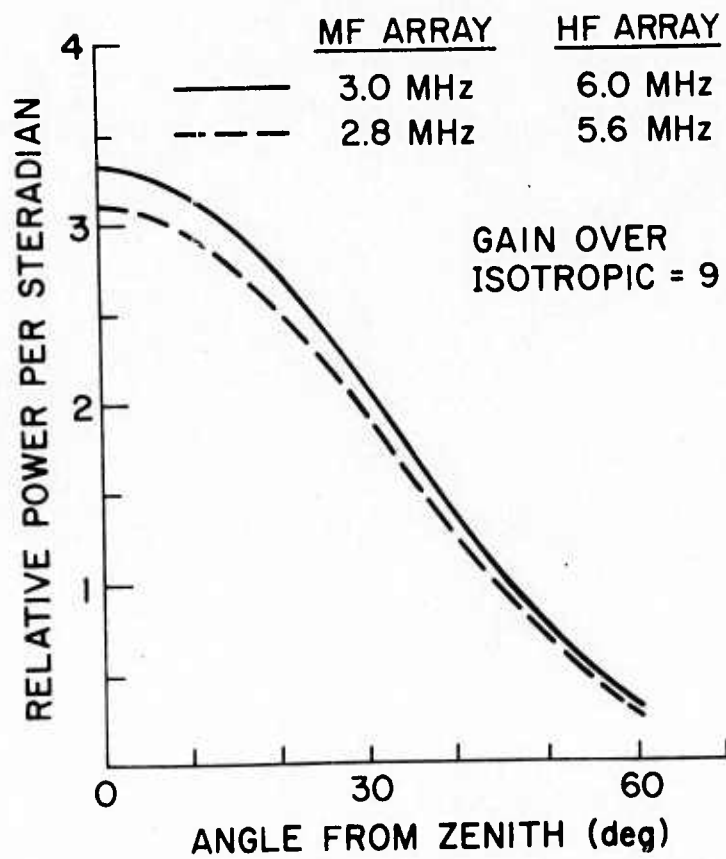


Figure 6.2 Antenna patterns. Single element (U)

SECRET

SECRET

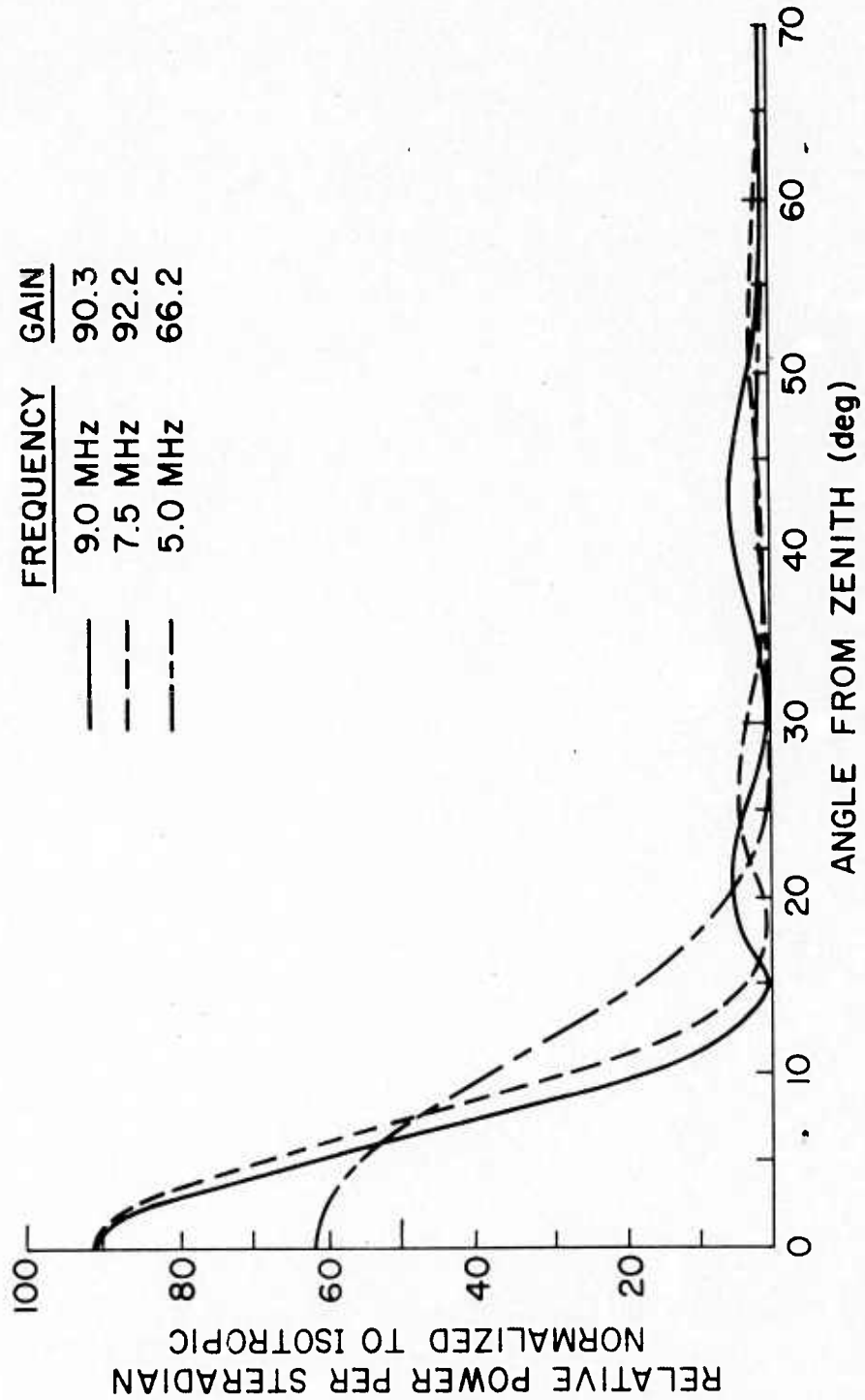


Figure 6.3 Antenna patterns. HF array, 0 deg tilt (U)

SECRET

SECRET

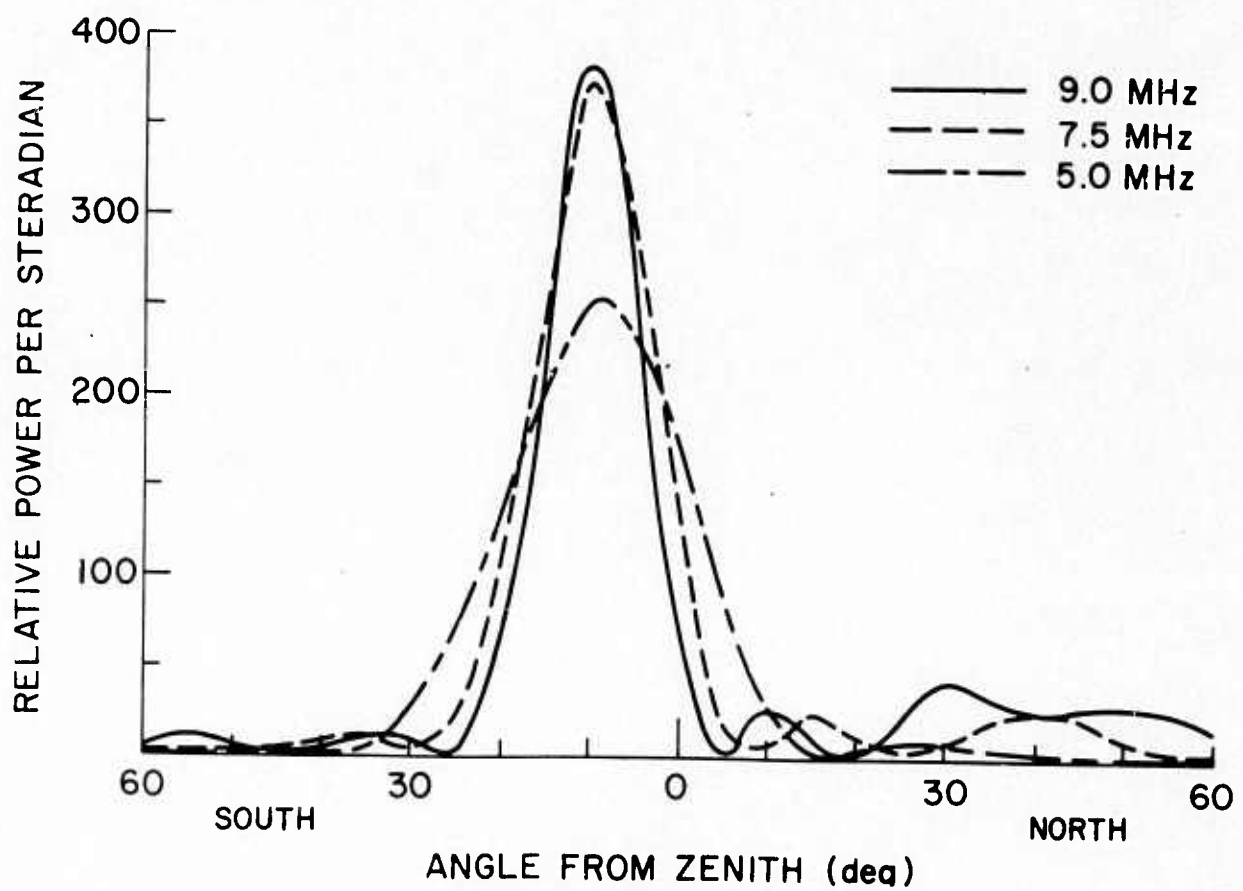


Figure 6.4 Antenna patterns. HF array, 10 deg tilt (U)

SECRET

SECRET

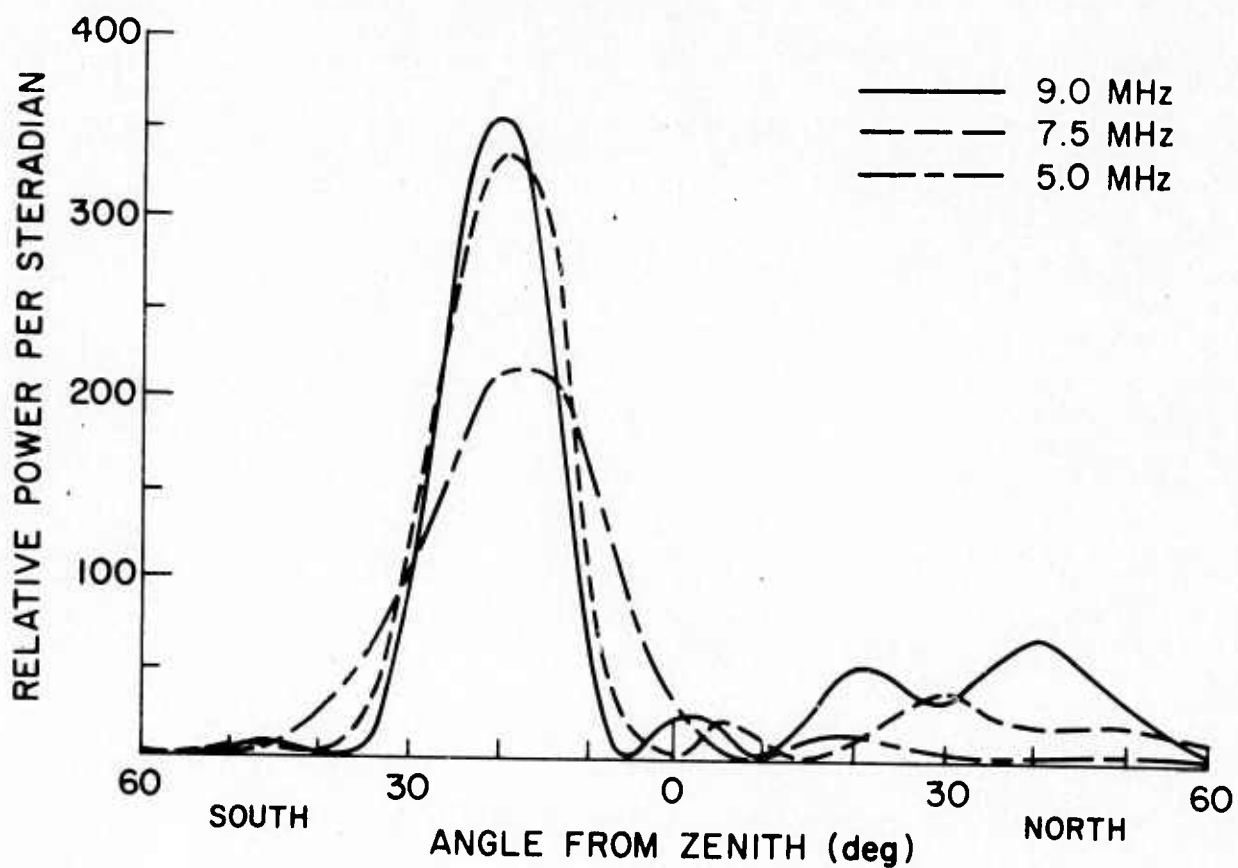


Figure 6.5 Antenna patterns. HF array, 20 deg tilt (U)

SECRET

SECRET

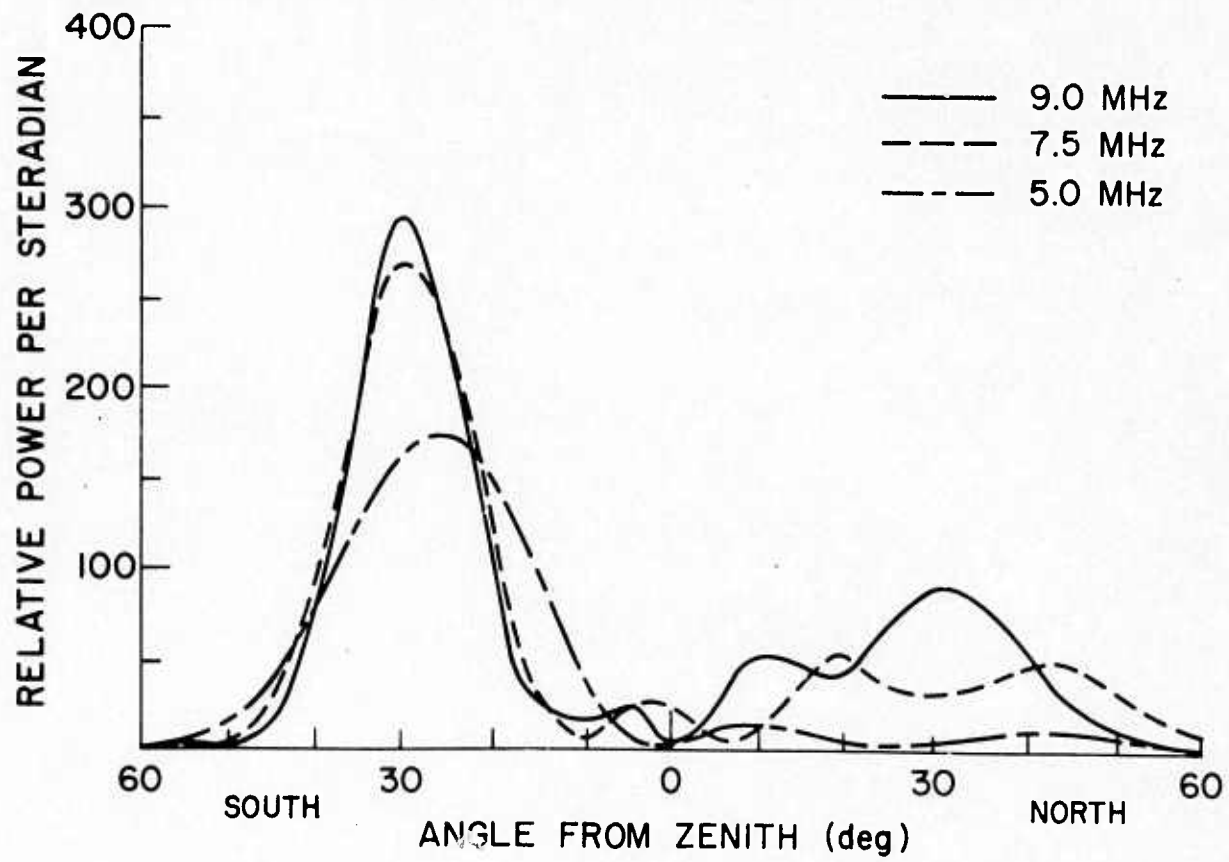


Figure 6.6 Antenna patterns. HF array, 30 deg tilt (U)

SECRET

SECRET

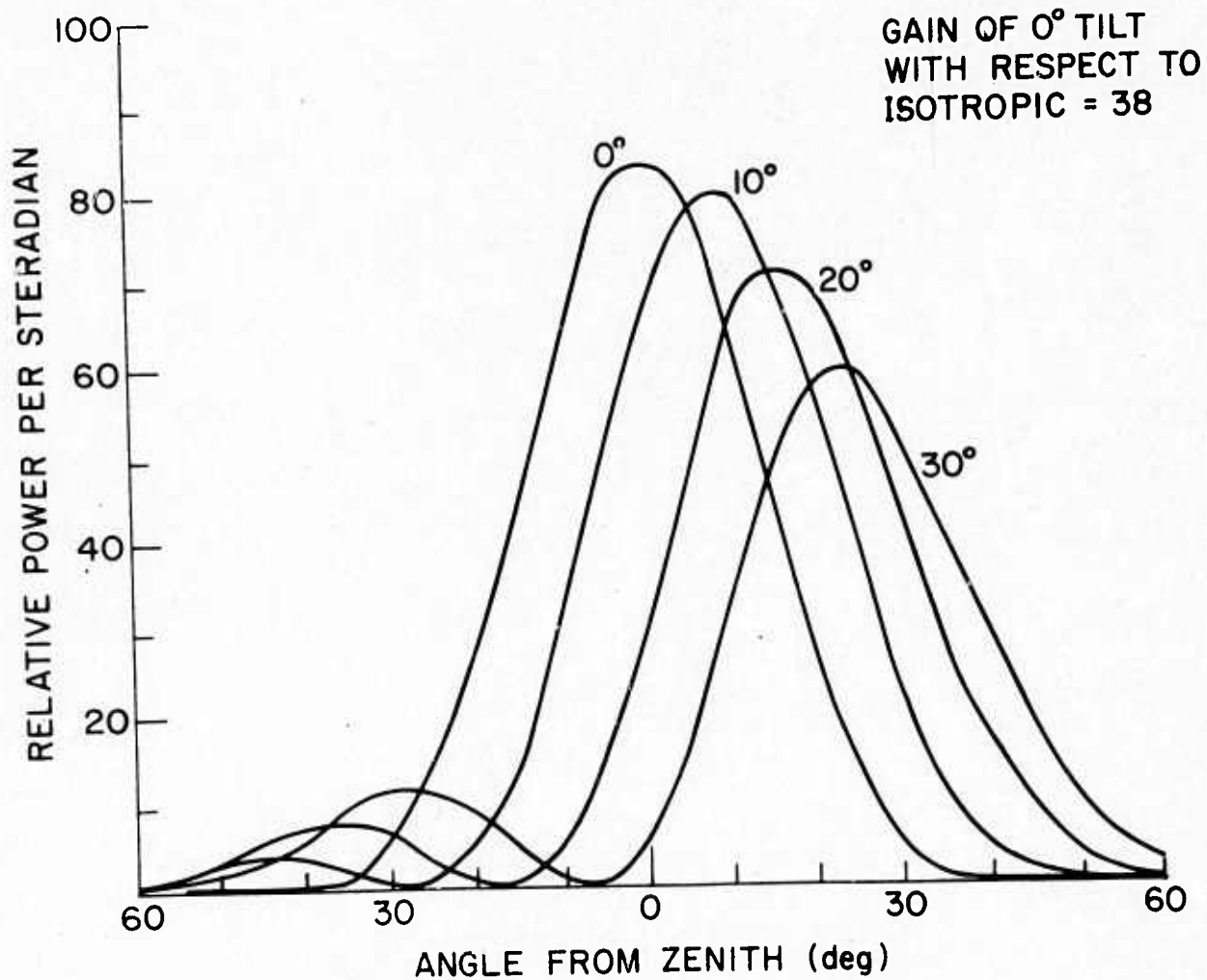


Figure 6.7 Antenna patterns. MF array, 3000 KHz (U)

SECRET

SECRET

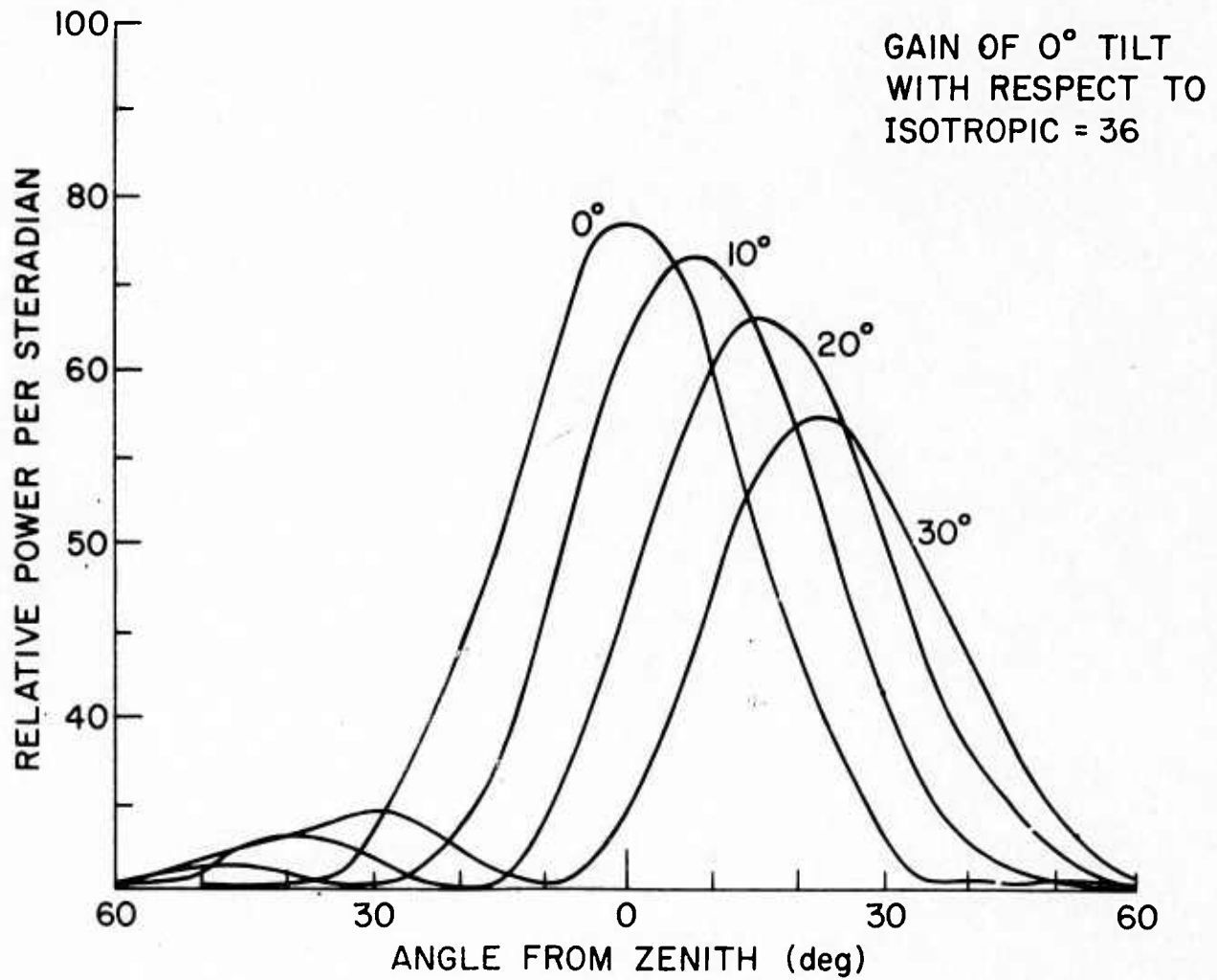


Figure 6.8 Antenna patterns. MF array, 2800 KHz (U)

SECRET

SECRET

Table 6.1

Summary of antenna array parameters

Array	Frequency	3 dB Main Lobe Beamwidth	Gain Over Isotropic	Relative Sidelobe Amplitude
Single Element	Mid-range	≈ 74 deg	≈ 9	None
HF	5.0 MHz	24 deg	66	-16 dB
HF	7.5 MHz	16 deg	92	-13 dB
HF	9.0 MHz	14 deg	90	-12 dB
MF	3.0 MHz	32 deg	38	small
MF	2.8 MHz	34 deg	36	small

SECRET

SECRET

of particular interest.

(S) Figure 6.2 gives the pattern of a single element. Since the height of the MF array elements are twice the height of the HF elements, a simple frequency scaling gives the pattern of both the MF and HF arrays.

(S) The pattern of the full 10-element HF array is shown in Figure 6.3. This figure has been scaled so that the scale is given with respect to an isotropic element. The sidelobes range from 20 to 30 degrees from the zenith.

(S) Figures 6.4, 6.5, and 6.6 comprise a study of the beam pattern as the main lobe is tilted at 10, 20, and 30 degrees toward the south. Actually, since the antenna has such axial symmetry, these patterns would be essentially the same for any azimuthal orientation of the tilt.

(S) Figures 6.7 and 6.8 were prepared from the antenna pattern of the MF array. The overall gain of the MF array with respect to an isotropic element is about 40 % that of the HF array.

(S) It can be seen from the figures that when the beam is tilted, the beamwidth increases somewhat, the gain is reduced, and the sidelobe amplitude is increased. Also of interest is that the pattern of an individual element (Figure 6.2) tends to "pull" the overall pattern toward the zenith when the beam is tilted. In this study, the antenna phases which were used to give a particular tilt were computed by assuming isotropic elements. When the phases were then used in the computation of the polar diagrams, the effect of the single element pattern caused some errors. These errors were less than 7 deg in the MF array (5 antennas) and less than 4 deg in the HF array (10 antennas).

6.3 Relative cross sections (U)

(S) The polar diagrams were next used in the calculations of relative cross sections. The basic computation was developed by Bowhill and Mendenhall (1972). This model assumed a displaced Gaussian shape for the north-south, east-west and vertical distribution of heater effect. The height distribution was centered at

SECRET

SECRET

the true height of reflection of the heater signal. The radar reflection point was calculated, and the radar cross section contribution at the reflection point was assumed to be linearly proportional to the heater effect.

(S) In the new version of this calculation the north-south and east-west variation of the heater power was computed from the antenna polar pattern. In order to calculate the relative cross section as a function of slant range from the radar site, it was necessary to integrate the cross section contribution along lines of constant slant range. These curves were then normalized to their maximum value.

(S) The result of these calculations is a set of curves of relative cross section as a function of slant range from the Stanford Research Institute radar. These curves have been normalized such that they equal one when the radar reflection point is that at the maximum of the heated region. Most of the curves do not satisfy this condition (i.e., they are mismatched), and thus have values considerably less than unity.

(S) Figures 6.9 through 6.17 are a study of the effect of various antenna beam tilts and configurations on the relative cross section curves. For all of this work, the radar site was chosen as the SRI site (range about 690 km, at about 10 deg W of magnetic south), and the e-folding distance in the z direction (i.e., the e-folding half-thickness of the heated region = A) was chosen as 10 km. This left only the heater signal reflection height and the heater antenna beam pattern as variables. For the SRI site, it can be shown that the optimum match between height of reflection and specular point occurs at a height of about 225 km if the beam is pointing straight up. This can be seen in most of the figures.

(S) Figure 6.9 is a study of the cross section as a function of height. It should be noted that the sidelobes become prominent at 240 and 245 km. This is caused by the fact that the north-tilted sidelobes are in a more favorable position to match this reflection height than the zenith-pointing main beam.

SECRET

SECRET

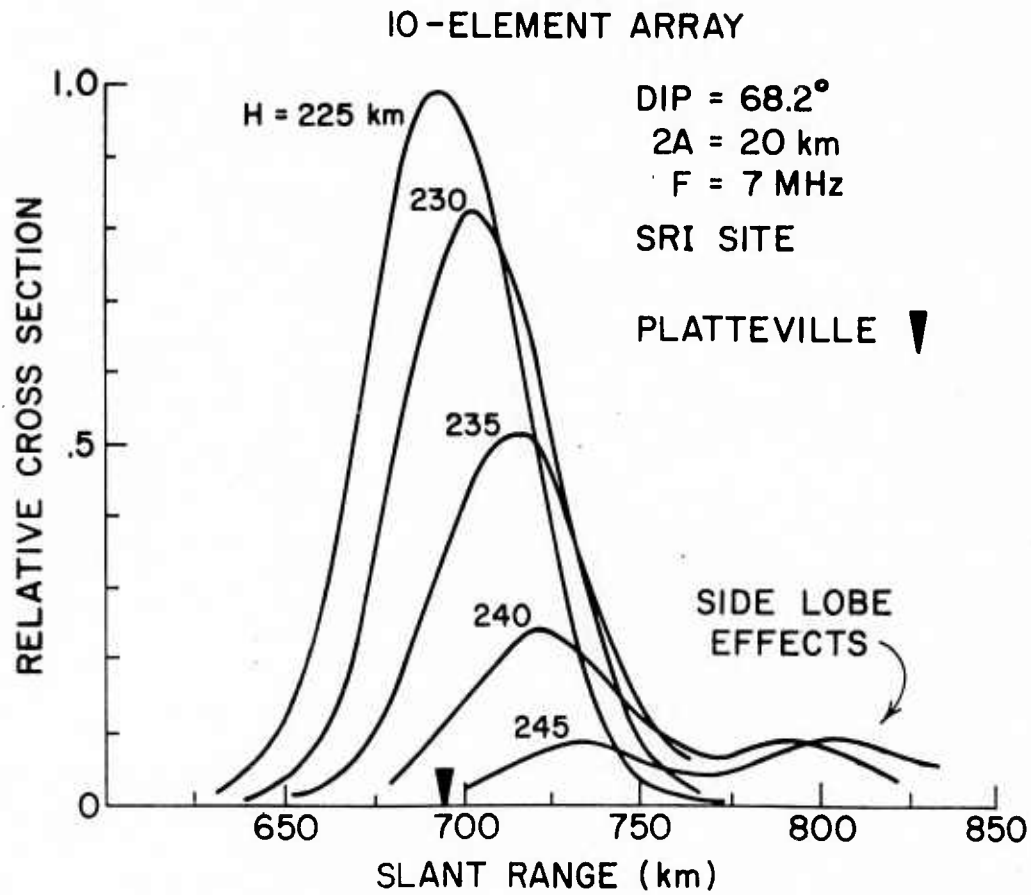


Figure 6.9 cross sections for various reflection heights (U)

SECRET

SECRET

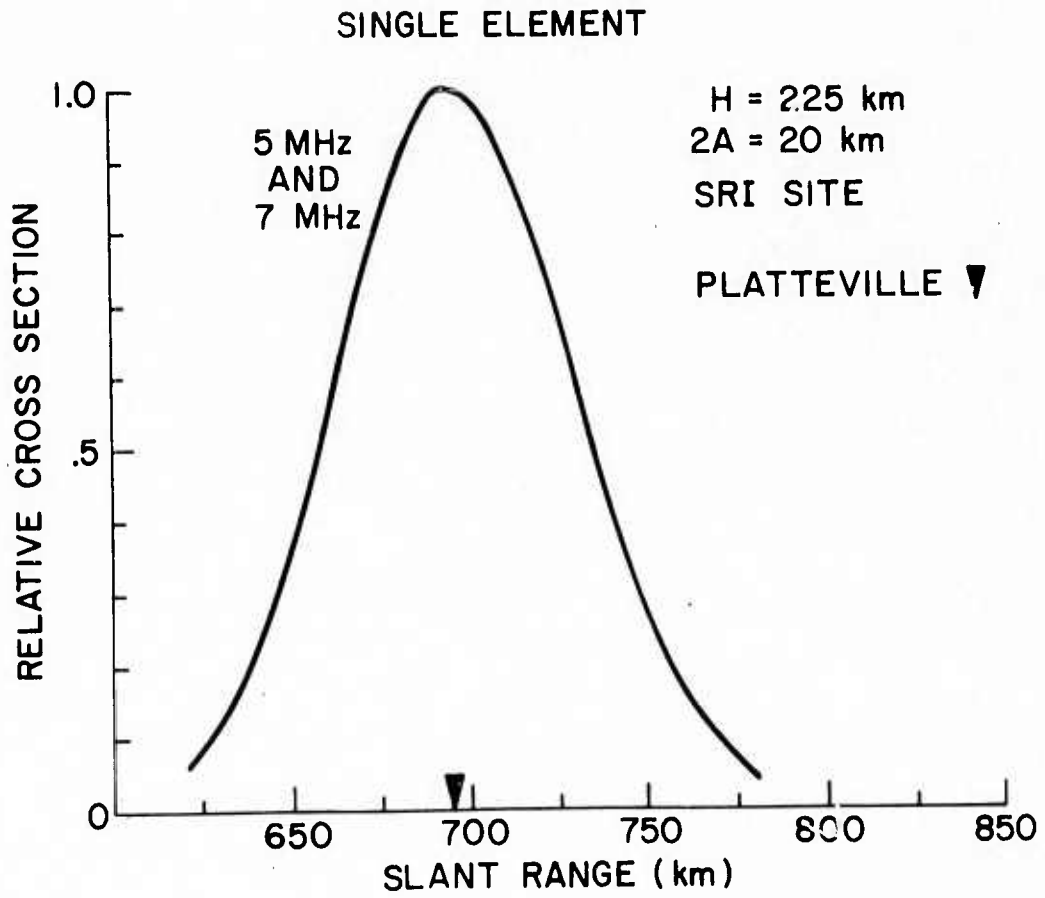


Figure 6.10 Cross section for single element (U)

SECRET

SECRET

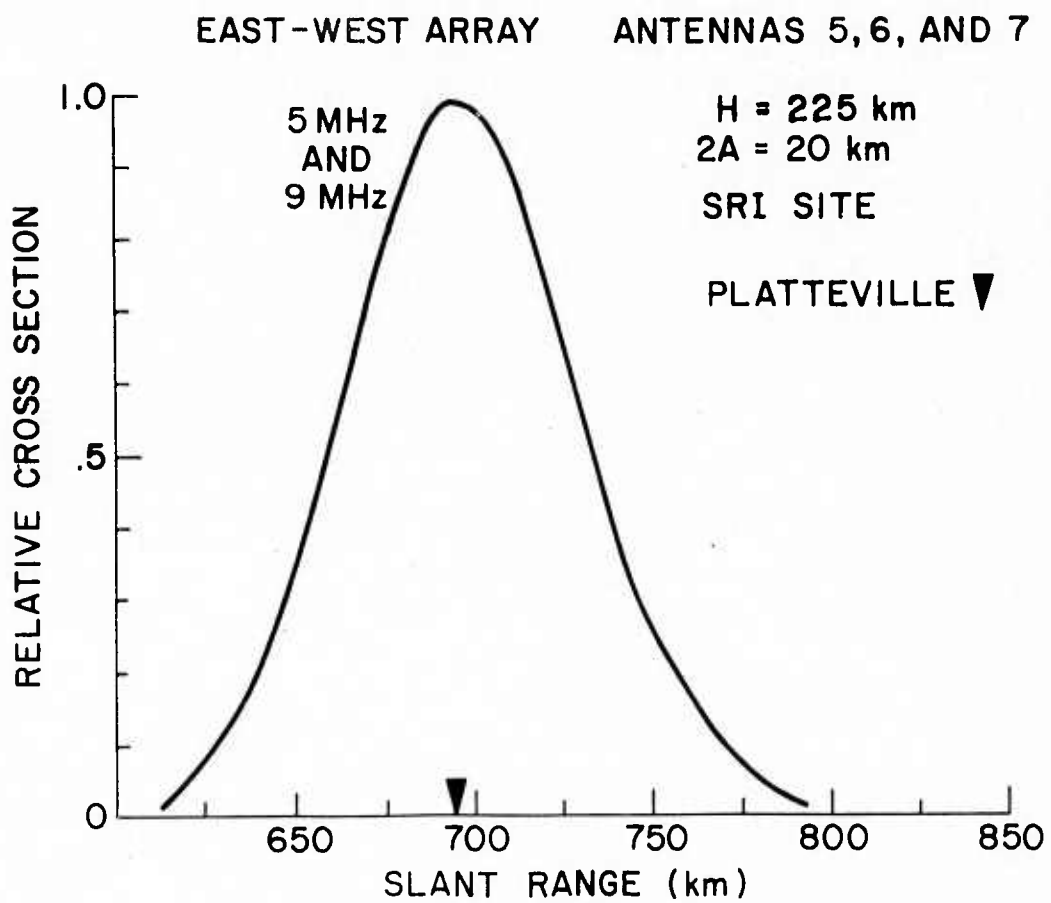


Figure 6.11 Cross section for E-W 3-element array (U)

SECRET

SECRET

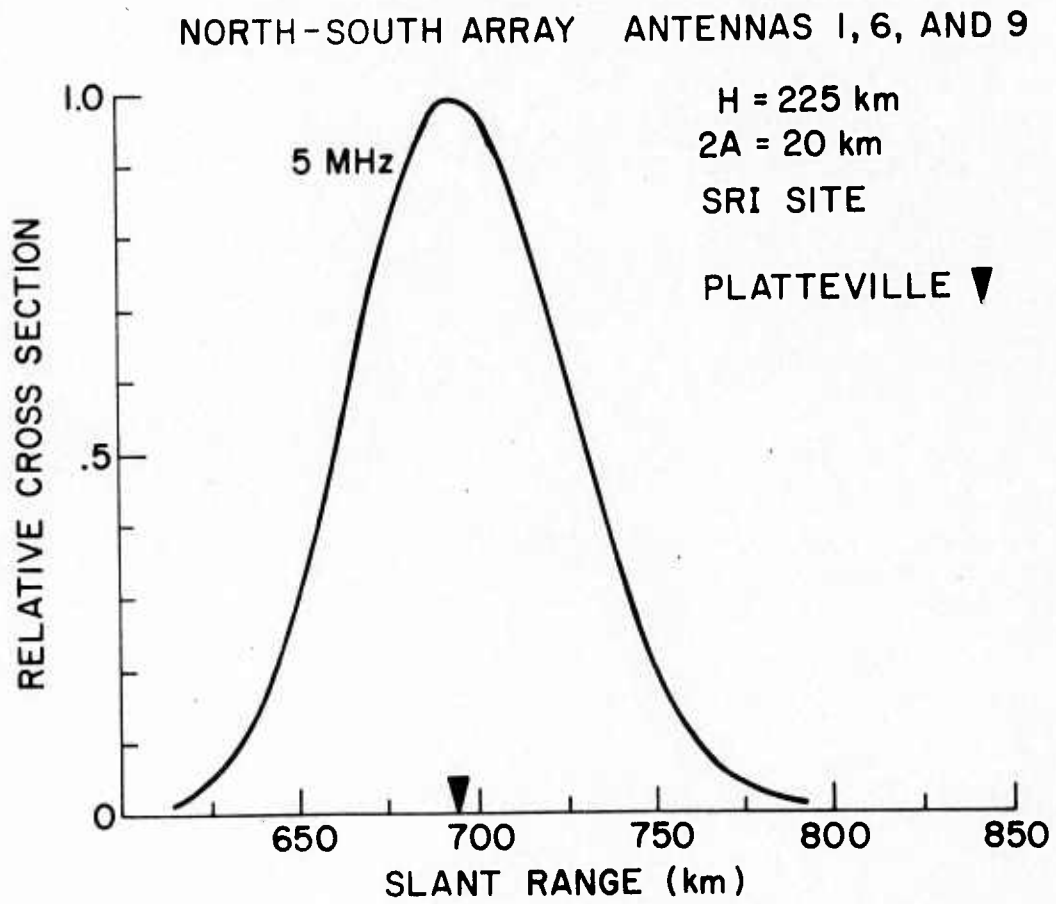


Figure 6.12 Cross section for N-S 3-element array (U)

SECRET

SECRET

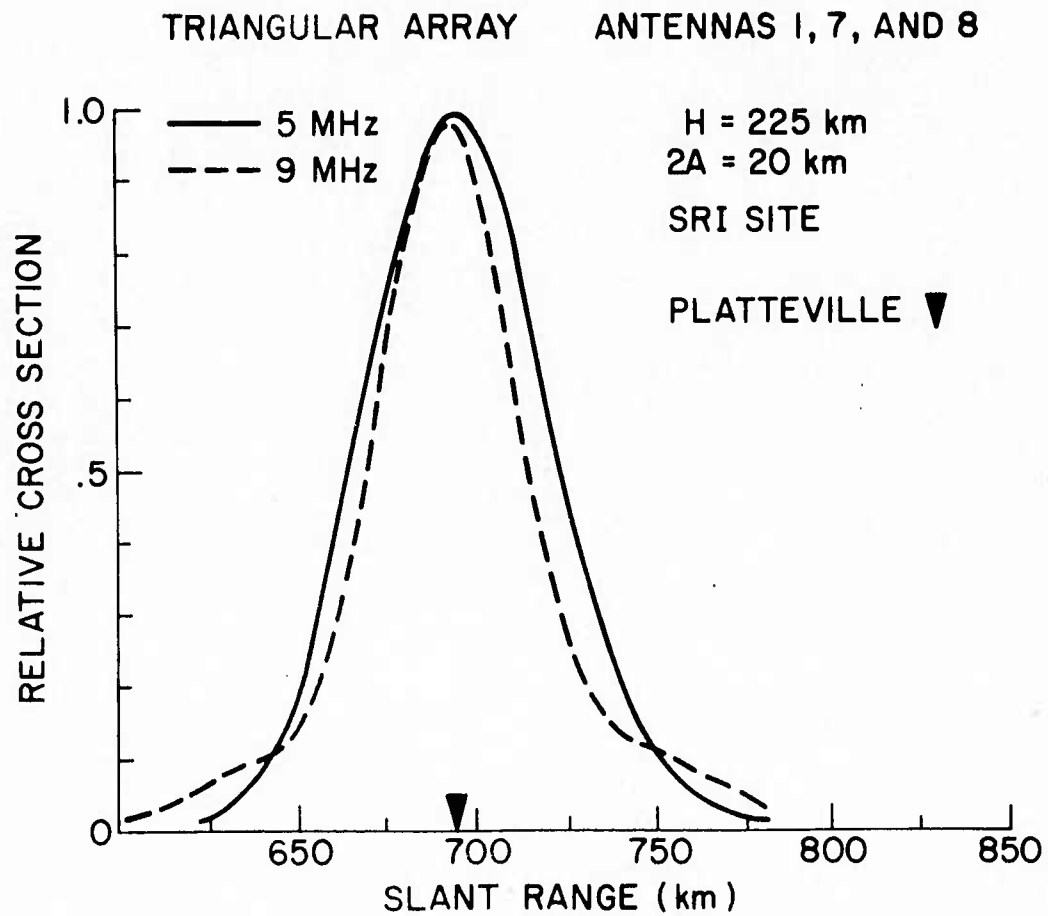


Figure 6.13 Cross section for triangular 3-antenna array (U)

SECRET

SECRET

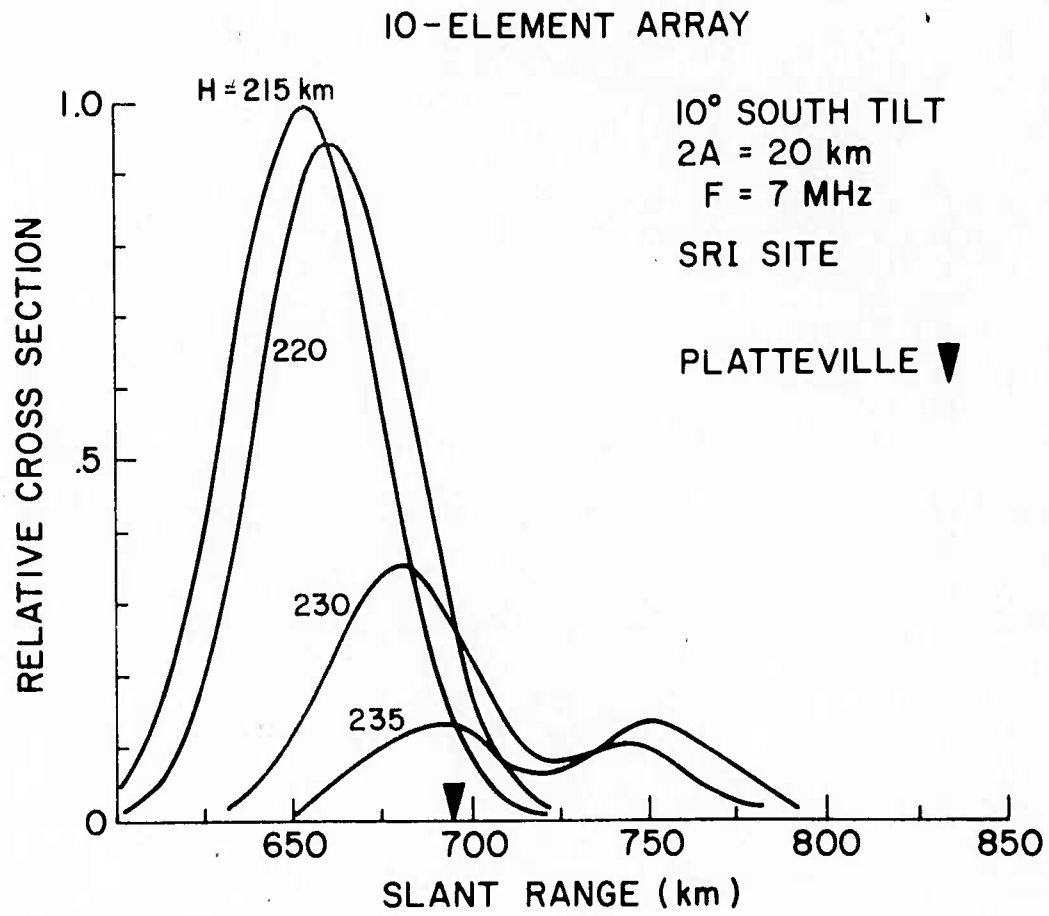


Figure 6.14 Cross sections for 10 deg south tilt (U)

SECRET

SECRET

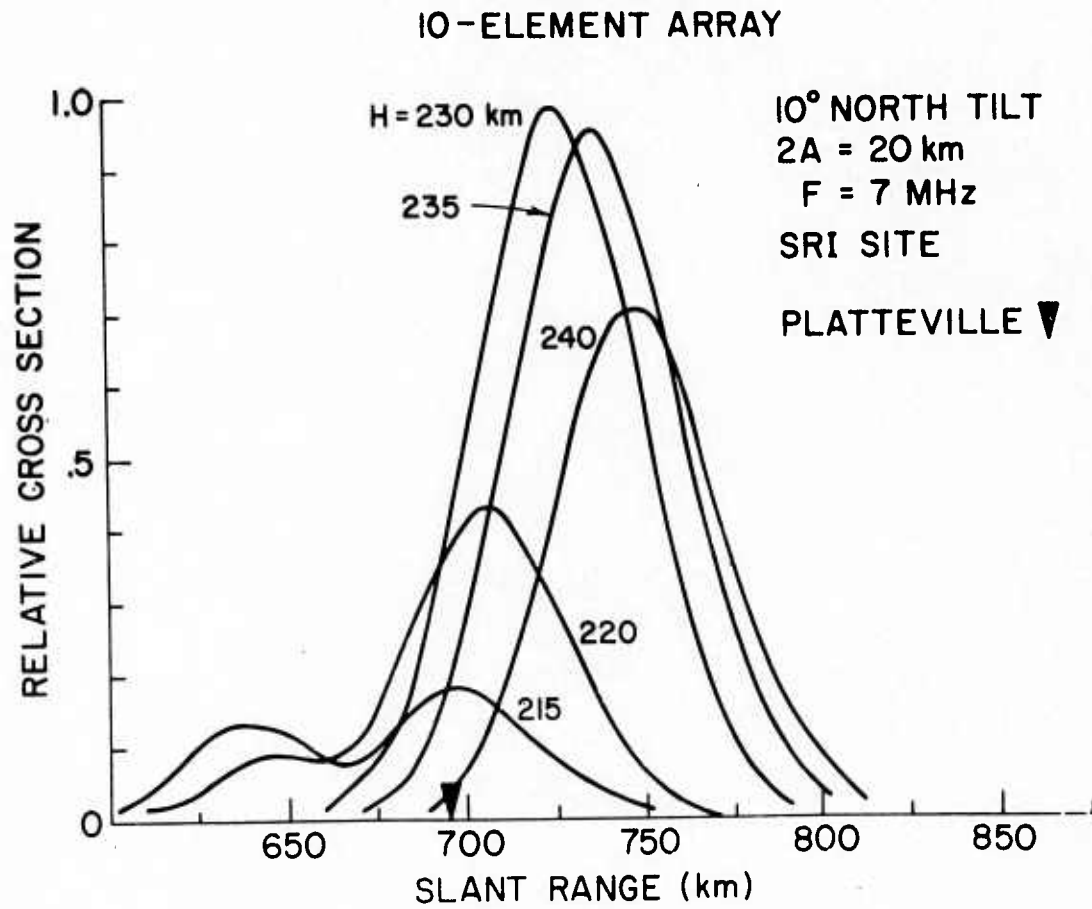


Figure 6.15 Cross sections for 10 deg north tilt (U)

SECRET

SECRET

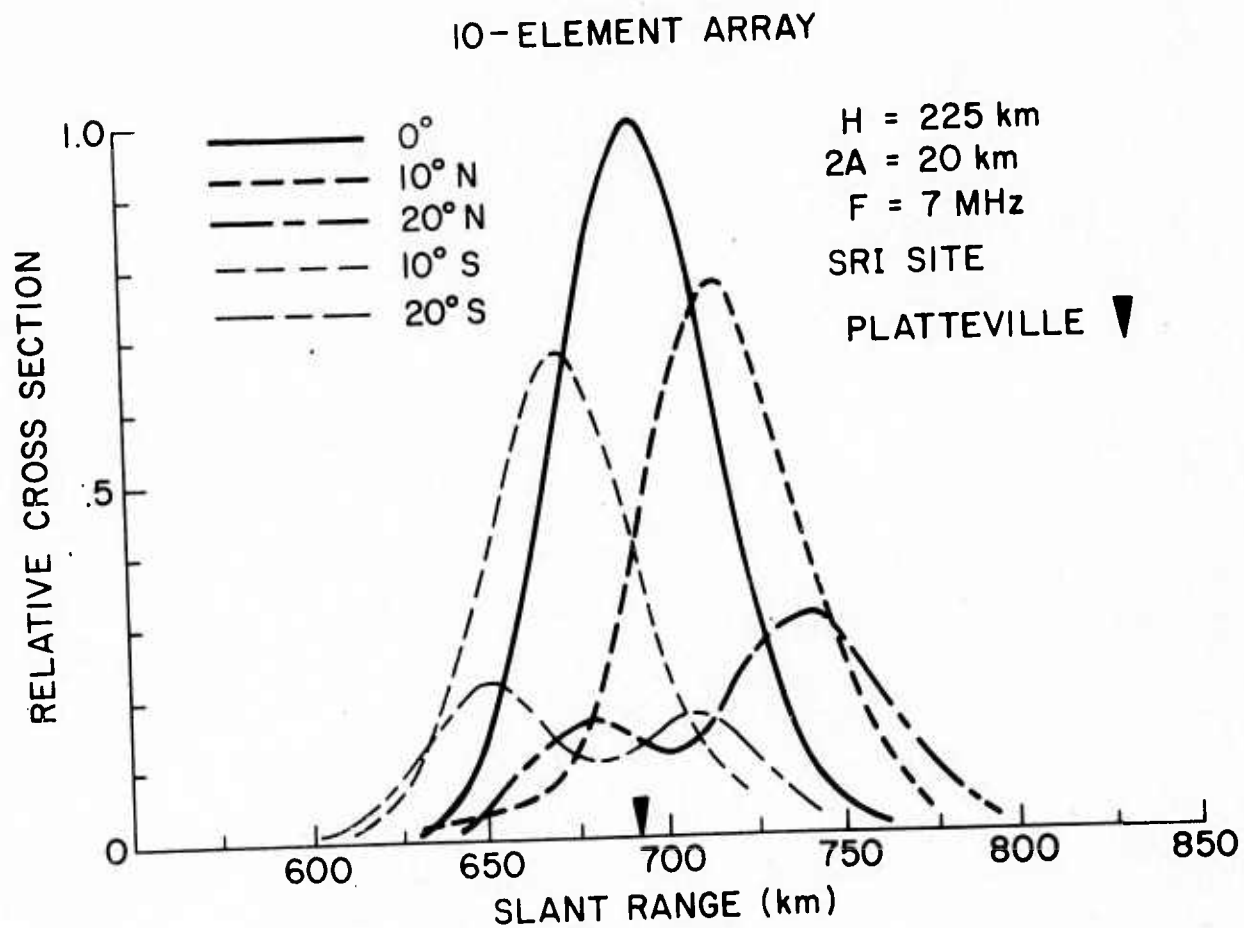


Figure 6.16 Cross sections for various tilt angles at a fixed reflection height of 225 km (U)

SECRET

SECRET

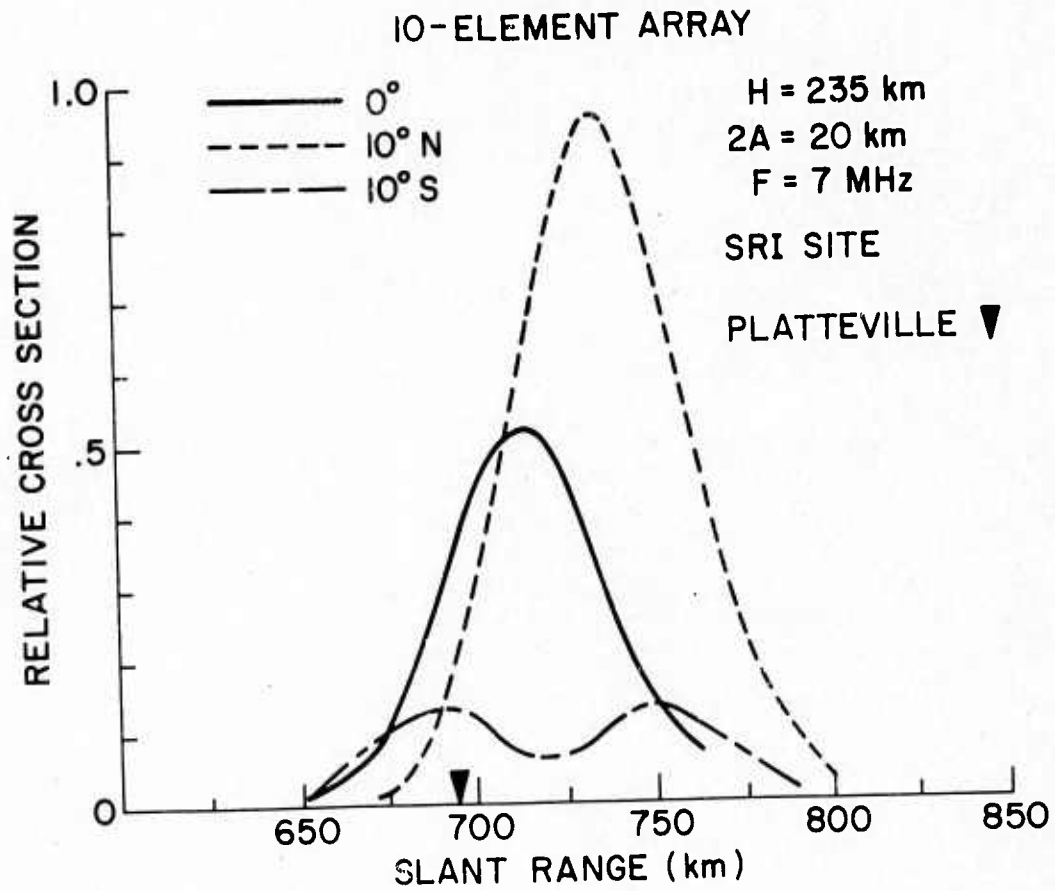


Figure 6.17 Cross sections for various tilt angles at a fixed reflection height of 235 km (U)

SECRET

SECRET

(S) Figures 6.10 through 6.13 show the variation of relative cross section for various antenna configurations. The fact that the peak value of these curves is approximately one is caused by the normalization scheme, and does not imply, for example, that the peak value of the cross section for a single element is necessarily the same as the value for 10 elements.

(S) The next set of figures concerns the effects of various beam tilts on the cross section. As can be seen in Figures 6.14 and 6.15, the tilt which gives the greatest cross section is about 10 deg south for a heater reflection height of 215 km and 10 deg north for a heater reflection height of 230 km. We have already mentioned that if the height is 225 km, the beam should be directly overhead. Figures 6.16 and 6.17 show the effect on the cross section when the height of reflection is held constant and the beam is tilted in various directions. Note in Figure 6.17 ($H = 235$ km) that the maximum cross section occurs when the beam is tilted 10 deg north. Once again it is clear that the sidelobes sometimes cause quite strong returns.

SECRET

UNCLASSIFIED

7. MODELS FOR D-REGION ABSORPTION

7.1 Introduction

This section describes some of the considerations that determine the ionospheric absorption of radio waves transmitted through the D region of the ionosphere. The absorption of a radio wave propagating vertically through the D region is primarily influenced by three factors; the frequency of the wave, the electron-density profile along the path, and the collision frequency profile.

7.2 Electron-density data

Because the electron density in the D region rises steeply with altitude above 80 km, there is not much absorption at lower altitudes. At altitudes above 90 km, the collision frequency drops off more rapidly than the electron density increases, so the absorption again diminishes.

Median electron densities in the ionosphere from 55 to 95 km at a solar zenith angle of 60 deg are shown in Table 7.1 (Mechtly, et al., 1972). Each profile is the median of five measured by a rocket technique (Mechtly, et al., 1967).

7.3 One-way absorption

In calculating the absorption, it is necessary to take note of three effects; the first of these is the variation of refractive index of the wave with altitude. This gives rise to a phenomenon of deviative absorption, which will be alluded to later. It is most prominent at the lower frequencies. The second effect is the polarization of the wave; the absorption coefficient for the extraordinary coefficient is larger than that for the ordinary by a ratio of approximately $(f + f_L)^2 / (f - f_L)^2$ where f is the wave frequency and f_L is the longitudinal component of the gyrofrequency (about 1.2 MHz). Thirdly, the Appleton-Hartree refractive index must be modified at altitudes below 80 km by

UNCLASSIFIED

UNCLASSIFIED

Table 7.1
Median-value profiles

km	Quiet sun cm ⁻³	Active sun cm ⁻³
95	1.33(4)	2.73(4)
94	1.11	2.01
93	9.13(3)	1.40
92	6.78	1.14
91	5.49	1.13
90	4.60	7.40(3)
89	3.69	6.86
88	2.84	7.40
87	2.07	5.40
86	1.38	4.89
85	6.40(2)	4.97
84	4.42	2.60
83	2.72	1.61
82	2.36	7.25(2)
81	2.36	7.70
80	1.98	7.09
79	2.17	6.82
78	2.36	5.85
77	2.11	5.18
76	1.86	4.63
75	1.79	4.07
74	1.79	4.36
73	1.29	4.10
72	1.35	3.23
71	1.16	2.38
70	9.44(1)	1.94
69	8.31	1.90
68	6.76	1.25
67	5.38	1.04
66	5.38	6.97(1)
65	4.36	5.10
64	3.75	5.41
63	4.56	3.76
62	3.14	2.58
61	2.94	1.45
60	2.94	8.96(0)
59	2.17	4.62
58	1.39	3.48
57	9.18(0)	3.95
56	7.60	3.03
55	4.29	2.51

() denotes multiplication by the enclosed power of 10.

UNCLASSIFIED

UNCLASSIFIED

the appropriate generalization (Sen and Wyller, 1960). All these effects have been taken into account in the calculations described below.

Electron densities and collision frequencies have been measured by the University of Illinois in a number of rocket flights, and those for solar zenith angle 60 deg have been used in Table 7.2 to compute one-way absorption through the D region at frequencies from 1.8 to 8.0 MHz. These include five flights in summer and equinox and eight flights in winter, when greater variability is expected. In all cases, the frequencies up to 3.0 MHz were reflected from the E layer, while those at 5 and 8 MHz were reflected from the F layer. Those observations in 1964-65-66 correspond to low sunspot activity; those in 68-69 to moderately high sunspot activity; and those in 71-73 to moderate sunspot activity.

These values of one-way absorption at 60 deg solar zenith angle (χ) can be related to absorptions at other values of χ by the fact that they are proportional to $\cos^{0.83} \chi$. Thus typical noon values at 40 deg latitude will be about 1.7 times those in Table 7.2, and early morning or late evening values will be proportionally less; so summer noon absorption may be about 4 dB at 5 MHz and 2 dB at 8 MHz.

The winter values are interesting. Although the solar zenith angle at noon in winter is about 60 deg at Wallops Island where these measurements were made, the absorptions at 5 and 8 MHz are almost as large as those observed in mid-summer, but with much greater variability (from 2.2 to 4.9 dB at 5 MHz, and from 1.0 to 2.2 dB at 8 MHz).

The figures for the absorption at frequencies of 3 MHz and below correspond to reflections from the E layer, and therefore are affected by deviative absorption. They are included in Table 7.2 to show how misleading absorption measurements below 3 MHz can be as indices of the absorption at higher frequencies. (Of course, vertical-incidence pulse absorption measures just twice the

UNCLASSIFIED

UNCLASSIFIED

Table 7.2
 Computed one-way vertical-incidence O-wave absorption, 60 deg solar zenith angle

<u>Season</u>	<u>1.8 MHz</u>	<u>2.1 MHz</u>	<u>2.4 MHz</u>	<u>2.7 MHz</u>	<u>3.0 MHz</u>	<u>5.0 MHz</u>	<u>8.0 MHz</u>	<u>3.0 MHz</u> Group Delay
Summer 65	1.1 dB	1.4 dB	1.5 dB	2.4 dB	14.5 dB	2.1 dB	1.0 dB	28.9 km
68	0.8	1.1	1.2	1.8	2.2	2.4	1.1	4.3
Equinox 64	1.4	1.5	2.0	6.7	11.9	1.8	0.9	23.8
65	1.2	1.4	1.6	1.5	1.1	1.3	0.6	2.2
69	1.4	1.1	1.2	1.4	8.2	2.4	1.1	16.3
Winter 65-6	0.4	0.3	0.3	0.3	0.3	2.4	1.0	0.5
65-6	0.7	1.9	1.4	1.7	1.3	4.9	2.2	2.5
67-8	0.9	1.0	1.7	1.4	2.0	2.4	1.1	4.0
68-9	1.9	1.5	1.7	2.2	2.3	3.6	1.6	4.6
68-9	0.4	1.6	1.8	2.0	2.5	3.2	1.5	4.9
71-2	0.6	0.7	2.0	2.5	3.6	3.1	1.4	7.1
72-3	0.3	0.3	2.2	2.7	5.7	2.2	1.0	11.4
72-3	0.4	0.3	0.3	0.3	0.3	2.4	1.0	6.3

UNCLASSIFIED

UNCLASSIFIED

absorptions given here.) For example, the highest absorption of all at 3 MHz was found on the summer 1965 rocket flight, with 14.5 dB one-way absorption, even though the 8 MHz absorption (1.0 dB) was one of the lowest. This is entirely due to deviative absorption, as can be seen from the final column in the table. This gives the calculated difference between group height and true height of reflection of a 3 MHz wave for that electron-density profile; this is proportional to the deviative absorption. The four rocket flights showing abnormally high (greater than 5 dB) absorption at 3 MHz frequency all have group delays exceeding 10 km.

In summer, the vertical incidence absorption A at 5 MHz at a latitude of 40 deg can be represented by the following formula:

$$A = B(2 \cos \chi)^{0.83}$$

where B is in the range 1.3 to 2.1 at sunspot minimum, and 2.2 to 2.4 at sunspot maximum. Individual winter values of B may be as high as 5 dB.

UNCLASSIFIED

SECRET

8. CONCLUSIONS (U)

8.1 Conclusions from scintillation measurements (U)

(S) The limited amount of geostationary scintillation data obtained in Prairie Smoke IV suggests that artificial spread F (ASF) formation disappears for heater frequency greater than about 98 % of the F2-layer critical frequency; that the scintillation index maximizes for heater frequency between 95 and 97 % foF2; and that within or below this range of heater frequencies, the scintillation yield is proportional to the heater power.

(S) Combined with the results of Prairie Smoke II, the 1/e correlation distance of the scintillations is found to lie for 80 % of the time between 75 and 300 m, and the velocity between 10 and 45 m/s in the east-west direction.

(S) The yield (in terms of scintillations) is highly variable. Scintillation indices ranging from 3.5 to 16 % can be seen over a period of 10 minutes or less when the modifier power and frequency as well as foF2 are constant (see Figure 3.2). A diurnal variation can be seen, the typical scintillation index measured during Prairie Smoke II varying from near 3 % at noon to better than 10 % at night. Finally, the data from Figure 3.2 seem to imply that the scintillation index is proportional to the square root of the modifier power.

(S) Digital correlation analysis of orbital satellite scintillation data from Prairie Smoke Ib and II has demonstrated the following:

1. ASF irregularities may be banana-shaped, curving upwards with altitude but oriented parallel to the magnetic field at the height of heater reflection.
2. Correlated scintillation due to structure sizes as small as 5 m is seen, its dimensions being about 1/15 of the large-scale structure size.

SECRET

SECRET

3. The disturbed region is quite patchy with regions of large and small structure interspersed.
4. Even with X-mode heating, small-scale structure is seen, though weaker than with O-mode heating.

8.2 Conclusions from OFS studies (U)

(S) A method of including the antenna polar diagram in the yield model has been developed. The purpose here has not been to propose an accurate yield versus power model, but to show the general variation of yield for different antenna tilt angles and array configurations. Any future and more accurate yield model should include these array polar diagram parameters as well as the tilted array parameters.

(S) One of the most interesting observations in this study is that the sidelobes of the antenna may cause effects with magnitudes even larger than that of the main lobe. This requires that the main lobe be "mismatched" while the sidelobe is "matched". Some of the experimental data seem to contain sidelobe effects. For example, the Proceedings of the Prairie Smoke IV RF Measurements Data Workshop (page 23) shows some data presented by Fialer and Frank (1973) which were collected at the SRI site in which a secondary echo is seen displayed about 100 km north of the main echo when the heater beam was pointed 20 deg south (height of reflection of heater signal = 233-238 km). These conditions are approximated by the 235 km curve of Figure 6.14 and by the 20 deg south curve of Figure 6.16. In both of these examples, a secondary echo about 60 km north of the main return is predicted.

(S) As a final point, the sidelobes could be exploited further. They seem quite useful as a diagnostic tool. A sidelobe actually produces a secondary heated region at the same time and in proximity to the primary heated region. The ratio of power delivered to these two regions can be estimated, and measurements

SECRET

SECRET

may be made on each. In fact, an experiment in which a specific sidelobe patten is deliberately generated to allow study of yield versus power could be easily implemented.

(S) Information on ranges of one-way absorption at 60 deg solar zenith angle has been presented and show that there may be a polarization factor at heater frequencies below 8 MHz.

SECRET

SECRET

9. REFERENCES (U)

- Bowhill, S. A. and E. E. Mendenhall, Procedures for determining scattering-model parameters (U), in Proceedings of the Prairie Smoke RF Scattering Model Workshop, 18, 19 July 1972 (U), pp 95-116, SRI 2-5209, Stanford Research Institute, Menlo Park, California (September 1972), SECRET.
- Bowhill, S. A., E. E. Mendenhall, and D. R. Ward (1972a), Transmission experiments in Prairie Smoke Ib and II (U), in Proceedings of Prairie Smoke II RF Measurements Data Workshop, 22, 23 June 1972 (U), pp 39-77, SRI 2-5388, Stanford Research Institute, Menlo Park, California (October 1972), SECRET.
- Bowhill, S. A., E. E. Mendenhall, and D. R. Ward (1972b), Transmission experiments in Prairie Smoke III (U), in Proceedings of Prairie Smoke III RF Measurements Data Workshop, 31 October 1972 (U), pp 47-64, SRI 3-4068, Stanford Research Institute, Menlo Park, California (January 1973), SECRET.
- Frank, V. R. and P. A. Fialer. (1973), Prairie Smoke IV SFCW observations (U), in Proceedings of the Prairie Smoke IV RF Measurements Data Workshop, 7 March 1973 (U), pp 5-36, SRI 3-4836, Stanford Research Institute, Menlo Park, California (June 1973), SECRET.
- Mechtly, E. A., S. A. Bowhill, and L. G. Smith (1972), Changes of lower ionosphere electron concentrations with solar activity, J. Atmos. Terr. Phys. 34, 1899-1907, UNCLASSIFIED.
- Mechtly, E. A., S. A. Bowhill, L. G. Smith, and H. W. Knoebel (1967), Lower ionosphere electron concentration and collision frequency from rocket measurements of Faraday rotation, differential absorption, and probe current, J. Geophys. Res. 72, 5239-5245, UNCLASSIFIED.

SECRET.

SECRET

Newman, P. (1966), Spread F and its effects upon radio wave propagation and communication, AGARDograph 95, Technivision, Maidenhead, England, pp 579-590, UNCLASSIFIED.

Sen, H. K. and A. A. Wyller (1960), On the generalization of the Appleton-Hartree magnetoionic formulas, J. Geophys. Res. 65, 3931-3950, UNCLASSIFIED.

Utlaut, W. F. (1970), An ionospheric modification experiment using very high power, high frequency transmission, J. Geophys. Res. 75, 6402-6405, UNCLASSIFIED.

SECRET

SECRET

SECURITY CLASSIFICATION OF THIS PAGE (When Data Entered)

REPORT DOCUMENTATION PAGE		READ INSTRUCTIONS BEFORE COMPLETING FORM
1. REPORT NUMBER RADC-TR-74-45	2. GOVT ACCESSION NO.	3. RECIPIENT'S CATALOG NUMBER
4. TITLE (and Subtitle) Experiments and Models in Prairie Smoke (U)		5. TYPE OF REPORT & PERIOD COVERED Final 1 Sep 71 31 Oct 73
		6. PERFORMING ORG. REPORT NUMBER
7. AUTHOR(s) S. A. Bowhill E. K. Walton D. R. Ward		8. CONTRACT OR GRANT NUMBER(s) F30602-72-C-0214
9. PERFORMING ORGANIZATION NAME AND ADDRESS Aeronomy Corporation P.O. Box 2209, Station A Champaign, IL 61820		10. PROGRAM ELEMENT, PROJECT, TASK AREA & WORK UNIT NUMBERS 14233002
11. CONTROLLING OFFICE NAME AND ADDRESS Defense Advanced Research Projects Agency 1400 Wilson Blvd. Arlington, VA 22209		12. REPORT DATE 15 Dec 1973
14. MONITORING AGENCY NAME & ADDRESS (if different from Controlling Office) Richard W. Carman (OCSE) RADC, GAFB, NY 13441		13. NUMBER OF PAGES 74
		15. SECURITY CLASS. (of this report) SECRET
15a. DECLASSIFICATION/DOWNGRADING SCHEDULE 3		
16. DISTRIBUTION STATEMENT (of this Report) None		
17. DISTRIBUTION STATEMENT (of the abstract entered in Block 20, if different from Report)		
18. SUPPLEMENTARY NOTES		
19. KEY WORDS (Continue on reverse side if necessary and identify by block number) Heated F Layer Morphology of Artificial Spread F		
20. ABSTRACT (Continue on reverse side if necessary and identify by block number) (S) This final report describes additional experiments to study the morphology of artificial spread F (ASF) irregularities by measuring the scintillation of VHF and UHF signals transmitted through the disturbed region from geostationary and orbital satellites. Scintillation depth, structure size and drift velocity measurements are described for Prairie Smoke IV, and are related to heater power. Detailed correlation analysis show		

DD FORM 1 JAN 73 1473

EDITION OF 1 NOV 65 IS OBSOLETE

SECRET

SECURITY CLASSIFICATION OF THIS PAGE (When Data Entered)

SECRET

SECURITY CLASSIFICATION OF THIS PAGE(When Data Entered)

the presence of a smaller structure in ASF of about 10 meter size. The results of these experiments are combined into a model for scintillation and spread F. The report also contains recommendations on the effect of antenna power patterns and beam steering on field-aligned VHF scatter; and on models for D-region absorption.

SECRET

SECURITY CLASSIFICATION OF THIS PAGE(When Data Entered)



MISSION
of
Rome Air Development Center

RADC is the principal AFSC organization charged with planning and executing the USAF exploratory and advanced development programs for electromagnetic intelligence techniques, reliability and compatibility techniques for electronic systems, electromagnetic transmission and reception, ground based surveillance, ground communications, information displays and information processing. This Center provides technical or management assistance in support of studies, analyses, development planning activities, acquisition, test, evaluation, modification, and operation of aerospace systems and related equipment.